Abstract

We study the effects of a meniscus on the oscillations of a viscous liquid filling a right circular cylindrical container by using the natural viscous complex eigenfunctions of the problem; the case of no-meniscus was considered in Kidambi(2007). The free surface of the liquid is assumed to have a pinned contact line. By projecting the governing equations onto an appropriate basis, a nonlinear eigenvalue problem for the complex frequencies is obtained. This is then solved to obtain the modal frequencies as a function of the contact angle θ_c, the Reynolds and Bond numbers Re and Bo and the liquid depth h . The effect of the meniscus is, in general, to decrease the modal frequency and increase (decrease) the damping rate according as $\theta_c < (>) 90^0$. However, there are parameter values for which the meniscus results in a frequency increase and anomalous behaviour in the damping rate. Extensive comparison with experimental (Howell et al 2000) and computational (Martel et al 1998, Nicolás 2002) results for the $\theta_c = 90^0$ case (Kidambi 2007) is very good; comparison with the one available experimental result of Cocciaro et al (1993) for $\theta_c = 62^0$ is also very good. Extensive results for a variety of contact angles have been tabulated for Reynolds and Bond numbers for which experimental results (Howell et al 2000) exist in the flat interface case, for comparison with future experimental results that may be obtained with curved menisci.

1 Introduction

This work seeks to determine the effects of a meniscus on the damping rate and frequency of linear surface waves in a circular cylinder of radius R. The determination of these quantities is a classical problem in fluid mechanics that not only has a history going back hundreds of years but which also has been studied extensively in recent times, a selection of the recent literature being Shankar (2007), Nicolás (2005), Nicolás (2002), Martel, Nicolás & Vega (1998), Miles & Henderson (1998), Henderson & Miles (1994) and Benjamin & Scott (1979). For each mode, the parameters influencing these two quantities are the gravitational Reynolds number ($Re = \sqrt{gR^3}/\nu$), the Bond number ($Bo = \rho g R^2/\sigma$), the liquid depth H and the contact angle θ_c. ρ, σ and ν are the density, surface tension and kinematic viscosity of the fluid and g is the acceleration due to gravity. Though a linear problem, it has been surprisingly hard to solve completely. The analytic approaches have almost exclusively, with the sole exception of the pioneering work of Nicolás (2002) which solves an eigenvalue problem, consisted of deriving asymptotic expressions for these two quantities with $Re^{-1/2}$ as the small expansion parameter. These calculations are tedious and have not been carried beyond $O(Re^{-1})$. The frequency at relatively high Re is predicted quite well by this approach, determined as it is by inviscid mechanisms in this regime; at low Re, the prediction deteriorates and is already off by almost 20% even for the not-so-low $Re \approx 300$ (Howell et al 2000). The damping rate is harder to predict because the sources of damping are various and hard to quantify, ranging as they do from the wall and free surface boundary layers to the moving contact line and surface contamination. The dynamics of the moving contact line is not particularly well understood and hence some workers going back to Benjamin & Scott (1979), have chosen to focus on the case of a pinned contact line; in particular, there has been a systematic effort to compare experimental values of the frequency and damping rate for various modes with theoretical values. Oscillations of the free surface in a brimful container and small free surface oscillations of very viscous liquid are two common situations where pinned contact lines may occur. Pinned contact lines have also been experimentally observed in a low-amplitude (Cocciaro, Faetti & Festa 1993) and a low-Reynolds number (Perlin, Schultz & Liu 2004) regime. The damping rates for the oscillations

with a pinned contact line are well predicted at high Re with the difference in experimental and analytic values often less than 5%. However, the comparison is not so good at the lower Re with errors in the $10 - 20\%$ range; moreover, the calculation to higher order will only worsen the error as positive terms add to the damping rate.

The pinned contact line problem, though simpler than the problem where the contact line moves, is nevertheless interesting and important because a) it allows a systematic study of the various factors affecting surface waves, singly and in combination, b) it is a clean linear problem whose solutions can be directly compared with experimental results, c) an understanding of the linear dynamics is essential to the building of a weakly nonlinear theory and d) it provides a solid foundation on which to base similar studies of the moving contact line problem. Till recently, the problem was considered only through the asymptotic approaches, which while providing valuable insights into the predominant sources of damping, have proved inadequate for low Re and high mode number regimes. Nicolás (2002), to our knowledge, is the only paper till now to formulate and solve an eigenvalue problem for the complex frequency for arbitrary values of Re. The method is based on the separation-of-variables technique and uses two sets of real eigenfunctions, one for the sidewall and one for the endwall and free surface. Nicolás' results are in good agreement with experimental values even in the low Re regime, thus bettering the asymptotic results.

However, almost all studies till now, both experimental and computational, have been for the case of a flat static free surface, the sole exceptions being an experimental study by Cocciaro et al (1992) wherein the damping rate and frequency in the pinned contact line regime have been measured for a $\theta_c = 62^0$ and one set of values of Re, Bo and h and computational studies by Shankar (2007) and Nicolás (2005) that take the meniscus into account but only in an inviscid analysis. In the rest of the literature, the contact angle θ_c is 90^0 and there is no meniscus. However, for real substances, the contact angle is almost never 90^0 and a meniscus is present. Still, for normal gravity conditions and containers with large dimensions, the meniscus is quite small with negligible effects. However, in microgravity conditions or in flows in containers of dimensions comparable to the capillary length, these effects can no longer be neglected and may even dominate. In these cases, quantifying the effects of a meniscus on the frequencies and damping rates becomes important. It is known from the work of Martel et al (1998) that the free surface boundary layer, for the case of $\theta_c = 90^0$, contributes to damping only at $O(Re^{-3/2})$. Though this results in an accurate enough value for large Re with only three terms (till $O(Re^{-1})$) it would increasingly be in error for $Re \to 0$. The situation is more uncertain when a meniscus is present. No studies similar to Martel et al (1998) exist for this case. Thus, it is not clear at what order the free surface contribution may become important and it is likely that the meniscus has an important role to play even at relatively large Reynolds number.

The present study seeks to fill this gap in the literature by formulating and solving an eigenvalue problem for the frequencies but with a meniscus present. The spirit of the work is the same as that in Nicolás (2002) with a semi-analytic solution based on the separation-of-variables method being used; the details, however are quite different. To start with, the present approach uses the natural eigenfunctions for the unsteady Stokes operator, introduced in Kidambi (2006) for calculating the unsteady Stokes flow in a cylindrical lid driven container, and these turn out to have complex eigenvalues which vary with the mode and Reynolds number. In contrast, Nicolás employs two sets of Fourier - Bessel eigenfunctions with fixed real eigenvalues. Each term in Nicolás' expansions cannot satisfy the no-slip boundary condition; in the present approach, the eigenvalues are found by requiring the satisfaction of this condition. The sidewall no-slip condition is satisfied only in the mean sense in Nicolás' approach thus making it unsuitable for an infinitely deep container. Though this is not a practical difficulty, it is a theoretical one which the present method does not face. Finally, Nicolás (2002) presented the method for the no-meniscus case and it is not clear how it generalises when a meniscus is present. This is because one of the eigenfunction sets used by Nicolás is defined on $[0, H]$ where H is

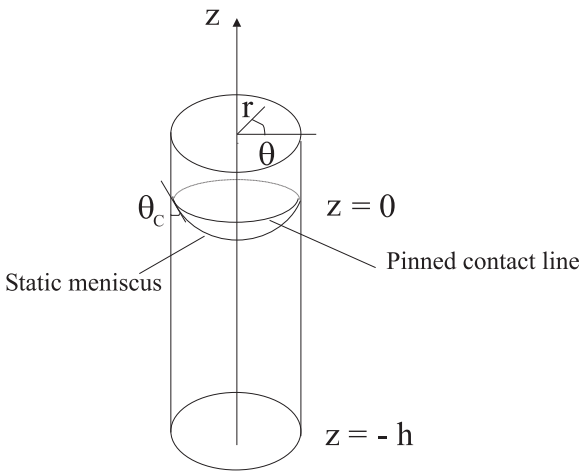

Figure 1: Geometry for oscillations of a free surface in a circular cylinder. The liquid is of depth h and the contact line is pinned.

the static liquid depth; in the presence of a meniscus, the static depth is variable and it is not clear how to proceed. The method presented in this paper does not suffer this limitation as the eigenfunctions are derived only from the satisfaction of the sidewall no-slip condition. A similar approach (Kidambi 2007) was used to calculate the frequency and damping rates for a two-dimensional rectangular geometry where the existence of a streamfunction simplifies matters. The present case is more difficult because a streamfunction does not exist and a vector potential has to be used.

The paper is organised as follows. §2 presents the governing equations and boundary conditions. §3 presents a solution of the problem which involves a) the computation of the static meniscus and b) an eigenvalue formulation and solution where the natural viscous complex eigenfunctions of the problem are used. §4 presents results for a range of Reynolds and Bond numbers; these include comparisons with published experimental (Cocciaro et al 1993) and computational (Nicolás 2005, Shankar 2007) results. Results are also presented for some of the experimental parameters of Howell et al (2000) but with a meniscus for possible comparisons with future experiments.

2 Governing equations

We consider the small oscillations of viscous liquid filling a circular cylindrical container of radius R. The static interface is assumed to make an arbitrary contact angle θ_c with the wall and the dynamic interface is assumed to have a pinned contact line i.e. the free surface displacement at the sidewall of the cylinder (figure 1) is zero. The liquid depth, H is measured as the distance between the bottom of the cylinder and the pinned contact line; we include the case when $H = \infty$. Scaling lengths by R and time by $\sqrt{R/g}$, and linearising around the rest state, we have (Johnson 1997)

$$\frac{\partial \hat{u}_r}{\partial r} + \frac{\hat{u}_r}{r} + \frac{1}{r}\frac{\partial \hat{u}_\theta}{\partial \theta} + \frac{\partial \hat{u}_z}{\partial z} = 0, \tag{1a}$$

$$\hat{\mathbf{u}}_t = -\nabla \hat{p} + \frac{1}{Re}\nabla^2 \hat{\mathbf{u}}, \tag{1b}$$

$$\hat{u}_r(r=1,\theta,z,t) = \hat{u}_\theta(r=1,\theta,z,t) = \hat{u}_z(r=1,\theta,z,t) = 0, \tag{1c}$$

$$\hat{u}_r(r,\theta,z=-h,t)=\hat{u}_\theta(r,\theta,z=-h,t)=\hat{u}_z(r,\theta,z=-h,t)=0 \text{ for the case of finite depth,} \tag{1d}$$

$$\hat{u}_r,\hat{u}_\theta,\hat{u}_z\to 0 \text{ as } \mathrm{z}\to-\infty, \text{ for the case of infinite depth,} \tag{1e}$$

$$\hat{\eta}_t+\eta_s^{'}\hat{u}_r=\hat{u}_z, \text{ on } \mathrm{z}=\eta_\mathrm{s}(\mathrm{r}), \tag{1f}$$

$$\left[\frac{\partial\hat{u}_r}{\partial z}+\frac{\partial\hat{u}_z}{\partial r}\right]\left[\eta_s^{'2}-1\right]+2\eta_s^{'}\left[\frac{\partial\hat{u}_r}{\partial r}-\frac{\partial\hat{u}_z}{\partial z}\right]=0, \text{ on } \mathrm{z}=\eta_\mathrm{s}(\mathrm{r}), \tag{1g}$$

$$\frac{\partial\hat{u}_\theta}{\partial z}+\frac{1}{r}\frac{\partial\hat{u}_z}{\partial\theta}-\eta_s^{'}\left(\frac{1}{r}\frac{\partial\hat{u}_r}{\partial\theta}-\frac{\hat{u}_\theta}{r}+\frac{\partial\hat{u}_\theta}{\partial r}\right)=0, \text{ on } \mathrm{z}=\eta_\mathrm{s}(\mathrm{r}), \tag{1h}$$

$$\hat{p}-\frac{2}{Re}\frac{1}{(1+\eta_s^{'2})}\left[\frac{\partial\hat{u}_z}{\partial z}+\eta_s^{'2}\frac{\partial\hat{u}_r}{\partial r}-\eta_s^{'}\left(\frac{\partial\hat{u}_r}{\partial z}+\frac{\partial\hat{u}_z}{\partial r}\right)\right]-\hat{\eta}$$
$$+\frac{1}{Bo}\left[\frac{1}{(1+\eta_s^{'2})^{3/2}}\frac{\partial^2\hat{\eta}}{\partial r^2}+\frac{\partial\hat{\eta}}{\partial r}\left(\frac{1+3\eta_s^{'2}}{r(1+\eta_s^{'2})^{3/2}}-\frac{3\eta_s^{'}\kappa_s}{1+\eta_s^{'2}}\right)+\frac{1}{r^2(1+\eta_s^{'2})^{1/2}}\frac{\partial^2\hat{\eta}}{\partial\theta^2}\right]=0 \text{ on } \mathrm{z}=\eta_\mathrm{s}(\mathrm{r}), \tag{1i}$$

$$\hat{\eta}(r=1,\theta,t)=0 \text{ and } \int_0^{2\pi}\int_0^1 \mathrm{r}\hat{\eta}(\mathrm{r},\theta,\mathrm{t})\mathrm{dr}\,\mathrm{d}\theta=0. \tag{1j,k}$$

Here $\hat{u}_r,\hat{u}_\theta$ and $\hat{u}_z$ are the r,θ and z components of velocity, $\hat{p}$ is the reduced pressure (with gravity incorporated), $Re=\sqrt{gR^3}/\nu$ is the gravitational Reynolds number and $Bo=\rho gR^2/\sigma$ is the Bond number. ρ, σ and ν are the density, surface tension and kinematic viscosity of the fluid and g is the acceleration due to gravity. The continuity equation is given by 1(a), the momentum equations by 1(b), the zero-velocity boundary conditions on the side wall by 1(c), the boundary condition on the bottom wall in the finite depth case by 1(d), the far-field condition in the infinite depth case by 1(e) and the kinematic, shear and normal stress conditions on the free surface $z=\eta_s(r)+\hat{\eta}(r,\theta,t)$ by 1(f,g,h,i). The static meniscus $z=\eta_s(r)$ satisfies the differential equation

$$\eta_s(r)=\frac{1}{Bo}\kappa_s(r)+\lambda_s, \text{ with } \kappa_\mathrm{s}(\mathrm{r})=\frac{\eta_\mathrm{s}^{''}+\eta_\mathrm{s}^{'}(1+\eta_\mathrm{s}^{'2})/\mathrm{r}}{(1+\eta_\mathrm{s}^{'2})^{3/2}} \tag{2a,b}$$

and $\eta_s^{'}(r=1)=\cot\theta_c$; the primes indicate differentiation with respect to r. Note that, under linearisation, 1(f,g,h,i) are applied on $z=\eta_s(r)$. The pinned contact line condition is given by 1(j) and the volume conservation condition by 1(k).

Anticipating the existence of axisymmetric modes, it may be noted that similar equations hold with the obvious change that there is no azimuthal dependence and that the velocity field is two-dimensional.

3 Solution

Since we are interested in oscillatory solutions to the system 1(a-k), we seek

$$\hat{u}_r(r,\theta,z,t)=\mathrm{e}^{\Omega t}u_r(r,\theta,z),\ \hat{u}_\theta(r,\theta,z,t)=\mathrm{e}^{\Omega t}u_\theta(r,\theta,z), \tag{3a,b}$$
$$\hat{u}_z(r,\theta,z,t)=\mathrm{e}^{\Omega t}u_z(r,\theta,z),\ \hat{p}(r,\theta,z,t)=\mathrm{e}^{\Omega t}p(r,\theta,z), \text{ and } \hat{\eta}(r,\theta,t)=\mathrm{e}^{\Omega t}\eta(r,\theta). \tag{3c,d,e}$$

where Ω is (the possibly complex) oscillatory frequency to be determined. Using 3(a-e) in system (1), we have

$$\frac{\partial u_r}{\partial r} + \frac{u_r}{r} + \frac{1}{r}\frac{\partial u_\theta}{\partial \theta} + \frac{\partial u_z}{\partial z} = 0, \tag{4a}$$

$$\Omega \mathbf{u} = -\nabla p + \frac{1}{Re}\nabla^2 \mathbf{u}, \tag{4b}$$

$$u_r(r=1,\theta,z) = u_\theta(r=1,\theta,z) = u_z(r=1,\theta,z) = 0, \tag{4c}$$

$$u_r(r,\theta,z=-h) = u_\theta(r,\theta,z=-h) = u_z(r,\theta,z=-h) = 0 \text{ for the case of finite depth,} \tag{4d}$$

$$u_r, u_\theta, u_z \to 0 \text{ as } z \to -\infty, \text{ for the case of infinite depth,} \tag{4e}$$

$$\Omega\eta = u_z - u_r \eta_s^{'}, \text{ on z} = \eta_\text{s}(\text{r}), \tag{4f}$$

$$\left[\frac{\partial u_r}{\partial z} + \frac{\partial u_z}{\partial r}\right]\left[\eta_s^{'2} - 1\right] + 2\eta_s^{'}\left[\frac{\partial u_r}{\partial r} - \frac{\partial u_z}{\partial z}\right] = 0, \text{ on z} = \eta_\text{s}(\text{r}), \tag{4g}$$

$$\frac{\partial u_\theta}{\partial z} + \frac{1}{r}\frac{\partial u_z}{\partial \theta} - \eta_s^{'}\left(\frac{1}{r}\frac{\partial u_r}{\partial \theta} - \frac{u_\theta}{r} + \frac{\partial u_\theta}{\partial r}\right) = 0, \text{ on z} = \eta_\text{s}(\text{r}), \tag{4h}$$

$$p - \frac{2}{Re}\frac{1}{(1+\eta_s^{'2})}\left[\frac{\partial u_z}{\partial z} + \frac{\partial u_r}{\partial r}\eta_s^{'2} - \eta_s^{'}\left(\frac{\partial u_r}{\partial z} + \frac{\partial u_z}{\partial r}\right)\right] - \eta$$
$$+\frac{1}{Bo}\left[\frac{1}{(1+\eta_s^{'2})^{3/2}}\frac{\partial^2 \eta}{\partial r^2} + \frac{\partial \eta}{\partial r}\left(\frac{1+3\eta_s^{'2}}{r(1+\eta_s^{'2})^{3/2}} - \frac{3\eta_s^{'}\kappa_s}{1+\eta_s^{'2}}\right) + \frac{1}{r^2(1+\eta_s^{'2})^{1/2}}\frac{\partial^2 \eta}{\partial \theta^2}\right] = 0 \text{ on z} = \eta_\text{s}(\text{r}), \tag{4i}$$

$$\eta(r=1,\theta) = 0 \text{ and } \int_0^{2\pi}\int_0^1 \text{r}\eta(\text{r},\theta)\text{dr dtheta} = 0. \tag{4j,k}$$

Following Kidambi(2006), we seek

$$\mathbf{u} = \nabla\phi + \nabla \times \mathbf{A}, \; p = -\Omega\phi \tag{5a,b}$$

where $\mathbf{B} = \nabla \times \mathbf{A}$ satisfies the vector Helmholtz equation, $\nabla^2\mathbf{B} = \Omega\, Re\, \mathbf{B}$, while ϕ satisfies $\nabla^2\phi = 0$. It is easily checked that the above velocity and pressure fields, with $\mathbf{B}$ and ϕ as defined satisfy the continuity and the linearised Navier-Stokes equations 4(a,b).

Using the results in Morse & Feshbach (1953), two independent solenoidal vector fields $\mathbf{B_1}$ and $\mathbf{B_2}$ satisfying the vector Helmholtz equation can be written as

$$\mathbf{B_1} = \mathrm{e}^{kz}\left[\mathbf{e_r}\begin{pmatrix}\cos m\theta \\ -\sin m\theta\end{pmatrix}\{J_{m-1}(\alpha r) + J_{m+1}(\alpha r)\} - \mathbf{e}_\theta\begin{pmatrix}\sin m\theta \\ \cos m\theta\end{pmatrix}\{J_{m-1}(\alpha r) - J_{m+1}(\alpha r)\}\right], \tag{6a}$$

$$\mathbf{B_2} = \mathrm{e}^{kz}\left[\mathbf{e_r}k\begin{pmatrix}\cos m\theta \\ -\sin m\theta\end{pmatrix}\{J_{m-1}(\alpha r) - J_{m+1}(\alpha r)\} - \mathbf{e}_\theta k\begin{pmatrix}\sin m\theta \\ \cos m\theta\end{pmatrix}\{J_{m-1}(\alpha r) + J_{m+1}(\alpha r)\}\right.$$
$$\left. +\mathbf{e_z}2\alpha\begin{pmatrix}\cos m\theta \\ \sin m\theta\end{pmatrix}J_m(\alpha r)\right]. \tag{6b}$$

Here, $(\mathbf{e_r}, \mathbf{e}_\theta, \mathbf{e_z})$ are the unit vectors in the cylindrical coordinate system, J_m is the Bessel function of the first kind of order m, and $\alpha = \sqrt{k^2 - \Omega Re}$. m and k are the azimuthal and axial wavenumbers. Note that out of the four possible vector fields given above, two generate radial and axial velocity fields that are symmetric about $\theta = 0$ and the other two antisymmetric. We shall call these 'symmetric' and 'antisymmetric' modes respectively as these correspond to

symmetric and antisymmetric free surface oscillations. However, the frequency of the mode with azimuthal wave number m is the same irrespective of whether it is symmetric or antisymmetric. From now on, we consider only symmetric modes, for definiteness. The scalar field ϕ can be immediately written down as

$$\phi(r,\theta,z) = \mathrm{e}^{kz}\begin{pmatrix}\cos m\theta\\ \sin m\theta\end{pmatrix} J_m(kr).$$

We now write down the velocity fields for the symmetric modes, with obvious changes for the antisymmetric ones. Anticipating imaginary eigenvalues, we scale the Bessel functions by an exponential factor $\exp(k_i)$, $k_i = \mathrm{Im(k)}$ to avoid the large numbers that result for Bessel functions of arguments with large imaginary parts. To avoid clutter in what follows, we suppress the scale with the understanding that $J_m(kr)$ actually means $J_m(kr)/\exp(k_i)$. By combining the fields $\nabla\phi, \mathbf{B_1}$ and $\mathbf{B_2}$ in the ratio 1:a:b, a candidate velocity field can be written as

$$v_r(r,\theta,z) = \mathrm{e}^{kz}\cos m\theta\left[\frac{\mathrm{d}}{\mathrm{dr}}J_m(kr) + a\{J_{m-1}(\alpha r) + J_{m+1}(\alpha r)\} + bk\{J_{m-1}(\alpha r) - J_{m+1}(\alpha r)\}\right], \tag{7a}$$

$$v_\theta(r,\theta,z) = -\mathrm{e}^{kz}\sin m\theta\left[\frac{m}{r}J_m(kr) + a\{J_{m-1}(\alpha r) - J_{m+1}(\alpha r)\} + bk\{J_{m-1}(\alpha r) + J_{m+1}(\alpha r)\}\right], \tag{7b}$$

$$v_z(r,\theta,z) = \mathrm{e}^{kz}\cos m\theta\left[kJ_m(kr) + b2\alpha J_m(\alpha r)\right]. \tag{7c}$$

The vanishing of the velocity on the sidewall $r = 1$ leads to the system of linear equations,

$$\frac{k}{2}\{J_{m-1}(k) - J_{m+1}(k)\} + a\{J_{m-1}(\alpha) + J_{m+1}(\alpha)\} + bk\{J_{m-1}(\alpha) - J_{m+1}(\alpha)\} = 0, \tag{8a}$$

$$mJ_m(k) + a\{J_{m-1}(\alpha) - J_{m+1}(\alpha)\} + bk\{J_{m-1}(\alpha) + J_{m+1}(\alpha)\} = 0, \tag{8b}$$

$$kJ_m(k) + b2\alpha J_m(\alpha) = 0. \tag{8c}$$

For (8) to have a non-trivial solution, we need

$$\begin{vmatrix} \frac{k}{2}\{J_{m-1}(k) - J_{m+1}(k)\} & J_{m-1}(\alpha) + J_{m+1}(\alpha) & k\{J_{m-1}(\alpha) - J_{m+1}(\alpha)\} \\ mJ_m(k) & J_{m-1}(\alpha) - J_{m+1}(\alpha) & k\{J_{m-1}(\alpha) + J_{m+1}(\alpha)\} \\ kJ_m(k) & 0 & 2\alpha J_m(\alpha) \end{vmatrix} = 0,$$

which, on simplification, leads to an eigenvalue relation for k which reads

$$\begin{aligned} 4k^2 J_{m-1}(\alpha)J_m(k)J_{m+1}(\alpha) + k\alpha J_m(\alpha)[J_{m-1}(k) - J_{m+1}(k)][J_{m-1}(\alpha) - J_{m+1}(\alpha)] \\ -4m^2 J_m(k)J_m^2(\alpha) = 0. \end{aligned} \tag{9}$$

For $k^\star$ and $\alpha^\star$ satisfying (9), Eqs. (7) will yield vector eigenfunctions provided the constants a and b are given by

$$a = \frac{mJ_m(k^\star)(1 - k^{\star 2}/\alpha^{\star 2})}{J_{m+1}(\alpha^\star) - J_{m-1}(\alpha^\star)},\ b = -\frac{k^\star}{2\alpha^\star}\frac{J_m(k^\star)}{J_m(\alpha^\star)}.$$

For $m \neq 0$, it is known from Kidambi (2006) that (9) has three sets of complex eigenvalues which we denote $\{\lambda_n\}, \{\mu_n\}$ and $\{\nu_n\}$. However, the equation in Kidambi (2006) is simpler than the present one because (9) involves the unknown Ω which has to be determined so as to satisfy an eigenvalue problem that we will derive in the next section.

We now sketch the solution for the axisymmetric modes($m = 0$), which is slightly different. For these modes, $\mathbf{B_2}$ (6(b)) is the only non-zero velocity field and is given by

$$\mathbf{B_2} = \mathrm{e}^{kz}[-\mathbf{e_r} k J_1(\alpha r) + \mathbf{e_z} \alpha J_0(\alpha r)].$$

A candidate velocity field can be written as

$$v_r(r,z) = -k\mathrm{e}^{kz}[J_1(kr) + 2bJ_1(\alpha r)],$$
$$v_z(r,z) = \mathrm{e}^{kz}[kJ_0(kr) + b2\alpha J_0(\alpha r)]$$

where the wave number k is a solution of the eigenvalue relation

$$\alpha J_1(k)J_0(\alpha) - kJ_0(k)J_1(\alpha) = 0, \text{ and } b = -\frac{k}{2\alpha}\frac{J_0(k)}{J_0(\alpha)}.$$

This eigenvalue equation has only two sets of complex eigenvalues $\{\lambda_n\}$ and $\{\mu_n\}$.

Before we go on to formulate an eigenvalue problem for Ω, we first briefly describe the calculation of the static meniscus in §3.1.

3.1 Computation of the static meniscus

The static meniscus $z = \eta_s(r)$ is computed by solving equation (2a), which is a two-point boundary-eigenvalue problem. The two boundary conditions are $\eta_s^{'}(1) = \cot\theta_c$ and $\eta_s^{'}(0) = 0$. With the coordinates fixed such that $\eta(1) = 0$ (pinned contact line), (2a) has solutions only for particular values of λ which is the eigenvalue. A convenient way to solve (2a) is to write η_s as

$$\eta_s(r) = \sum_{n=1}^{N} u_m[\cos k_m r + (-1)^m \frac{k_m}{2}(1-r^2)] - \frac{\cot\theta_c}{2}(1-r^2)$$

where $k_m = (2m-1)\pi/2$ and the coefficients u_m are obtained by a least squares error minimisation procedure. Note that the boundary conditions are satisfied by the assumed form for $\eta_s(r)$.

The minimisation procedure consists of the following steps -

1. First write 2(a) as

$$\eta_s(r) - \frac{1}{Bo}[\eta_s^{''} + \frac{\eta_s^{'}}{r}] - \lambda_s = \frac{1}{Bo}\left[\eta_s^{''}\left(\frac{1}{(1+\eta_s^{'2})^{3/2}} - 1\right) + \frac{\eta_s^{'}}{r}\left(\frac{1}{(1+\eta_s^{'2})^{1/2}} - 1\right)\right]$$

   and consider N equally spaced points $r_i = i/(N-1), i = 0, 1, \cdots N$ over which the error in the above equation will be minimised.

2. Define the error at the i^{th} point e_i as

$$e_i = \eta_s(i) - \frac{1}{Bo}[\eta_s^{''}(i) + \frac{\eta_s^{'}(i)}{r_i}] - \lambda_s - rhs(i)$$

   where $rhs(i)$ is the right hand side of the equation in step (1) evaluated at the i^{th} point.

3. Consider the total squared error E_t defined as

$$E_t = \sum_{i=1}^{N} e_i^2.$$

The coefficients u_m are obtained by minimising E_t with respect to u_m i.e. by setting $\partial E_t/\partial u_m = 0, m = 1, \cdots N$ and solving the resulting system of linear equations. Finally, the eigenvalue λ is obtained from

$$\lambda = \frac{1}{Bo}\left[(\sum_{n=1}^{N} u_n k_n (-1)^n - \cot\theta_c)\sin^3\theta_c - \cos\theta_c\right].$$

3.2 The case of infinite depth

We will first sketch the solution for the simpler case of an infinitely deep container. We write the three components of the velocity field u_r, u_θ and u_z as linear combinations of the vector eigenfunctions given in (7). Denoting

$$p_n^1(r) = \left[\frac{\mathrm{d}}{\mathrm{dr}} J_m(\lambda_n r) + a\{J_{m-1}(\alpha_n^1 r) + J_{m+1}(\alpha_n^1 r)\} + b\lambda_n\{J_{m-1}(\alpha_n^1 r) - J_{m+1}(\alpha_n^1 r)\}\right], \quad (10a)$$

$$p_n^2(r) = \left[\frac{m}{r} J_m(\lambda_n r) + a\{J_{m-1}(\alpha_n^1 r) - J_{m+1}(\alpha_n^1 r)\} + b\lambda_n\{J_{m-1}(\alpha_n^1 r) + J_{m+1}(\alpha_n^1 r)\}\right], \quad (10b)$$

$$p_n^3(r) = \left[\lambda_n J_m(\lambda_n r) + 2b\alpha_n^1 J_m(\alpha_n^1 r)\right], \quad (10c)$$

$$q_n^1(r) = \left[\frac{\mathrm{d}}{\mathrm{dr}} J_m(\mu_n r) + a\{J_{m-1}(\alpha_n^2 r) + J_{m+1}(\alpha_n^2 r)\} + b\mu_n\{J_{m-1}(\alpha_n^2 r) - J_{m+1}(\alpha_n^2 r)\}\right], \quad (10d)$$

$$q_n^2(r) = \left[\frac{m}{r} J_m(\mu_n r) + a\{J_{m-1}(\alpha_n^2 r) - J_{m+1}(\alpha_n^2 r)\} + b\mu_n\{J_{m-1}(\alpha_n^2 r) + J_{m+1}(\alpha_n^2 r)\}\right], \quad (10e)$$

$$q_n^3(r) = \left[\mu_n J_m(\mu_n r) + 2b\alpha_n^2 J_m(\alpha_n^2 r)\right], \quad (10f)$$

$$s_n^1(r) = \left[\frac{\mathrm{d}}{\mathrm{dr}} J_m(\nu_n r) + a\{J_{m-1}(\alpha_n^3 r) + J_{m+1}(\alpha_n^3 r)\} + b\nu_n\{J_{m-1}(\alpha_n^3 r) - J_{m+1}(\alpha_n^3 r)\}\right], \quad (10g)$$

$$s_n^2(r) = \left[\frac{m}{r} J_m(\nu_n r) + a\{J_{m-1}(\alpha_n^3 r) - J_{m+1}(\alpha_n^3 r)\} + b\nu_n\{J_{m-1}(\alpha_n^3 r) + J_{m+1}(\alpha_n^3 r)\}\right], \quad (10h)$$

$$s_n^3(r) = \left[\nu_n J_m(\nu_n r) + 2b\alpha_n^3 J_m(\alpha_n^3 r)\right], \quad (10i)$$

we can write the three components of the velocity field for the m^{th} azimuthal mode as

$$u_r(r,\theta,z) = \cos m\theta \sum_{n=1}^{N}\left[a_n p_n^1(r) e^{\lambda_n z} + b_n q_n^1(r) e^{\mu_n z} + c_n s_n^1(r) e^{\nu_n z}\right], \quad (11a)$$

$$u_\theta(r,\theta,z) = -\sin m\theta \sum_{n=1}^{N}\left[a_n p_n^2(r) e^{\lambda_n z} + b_n q_n^2(r) e^{\mu_n z} + c_n s_n^2(r) e^{\nu_n z}\right], \quad (11b)$$

$$u_z(r,\theta,z) = \cos m\theta \sum_{n=1}^{N}\left[a_n p_n^3(r) e^{\lambda_n z} + b_n q_n^3(r) e^{\mu_n z} + c_n s_n^3(r) e^{\nu_n z}\right], \quad (11c)$$

where only the eigenvalues with positive real part are included as the field has to decay at infinity. In the above, $\alpha_n^1 = \sqrt{\lambda_n^2 - \Omega Re}, \alpha_n^2 = \sqrt{\mu_n^2 - \Omega Re}, \alpha_n^3 = \sqrt{\nu_n^2 - \Omega Re}$ (these appear in p_n^j, q_n^j and $s_n^j, j = 1, 2, 3$); a_n, b_n, c_n are the unknown complex coefficients that have to be determined such that the remaining boundary conditions 4(f,g,h,i), which also contain the unknown frequency Ω, are satisfied. We now obtain an eigenvalue problem for Ω; the eigenvectors will give the a_n, b_n and c_n. We follow a weighted residual method approach and require the inner product of equations 4(g,h,i) with the first N members of a complete set of test functions to vanish. We choose the test functions as the set $\{J_m(\delta_l r), l = 1, 2, \cdots\}$, where the δ_l are the roots of J_m. First we project the shear stress conditions on the interface 4(g,h) onto this set of functions $\{J_m(\delta_l r), l = 1, 2, \cdots\}$ to obtain the system of equations

$$\sum_{n=1}^{N}(a_n\beta_{nl}^1 + b_n\xi_{nl}^1 + c_n\chi_{nl}^1) = 0, \text{ and} \tag{12a}$$

$$\sum_{n=1}^{N}(a_n\beta_{nl}^2 + b_n\xi_{nl}^2 + c_n\chi_{nl}^2) = 0. \tag{12b}$$

The expressions for the integrals appearing in (12) are given in Appendix A. (12) can be written in matrix form as

$$\mathbf{X_1 a} + \mathbf{Y_1 b} + \mathbf{Z_1 c} = 0,$$
$$\mathbf{X_2 a} + \mathbf{Y_2 b} + \mathbf{Z_2 c} = 0$$

from which $\mathbf{b}$ and $\mathbf{c}$ can be expressed in terms of $\mathbf{a}$ as

$$\mathbf{b} = -\mathbf{U_2}^{-1}\mathbf{U_1 a}, \ \mathbf{c} = -\mathbf{Z_1}^{-1}(\mathbf{X_1 a} + \mathbf{Y_1 b}) \tag{13a,b}$$

where $\mathbf{U_1} = \mathbf{X_2} - \mathbf{Z_2 Z_1}^{-1}\mathbf{X_1}$, and $\mathbf{U_2} = \mathbf{Y_2} - \mathbf{Z_2 Z_1}^{-1}\mathbf{Y_1}$.

Equations 4(f) and 4(i) involve $\eta(r, \theta)$ which we seek as

$$\eta(r, \theta) = \cos m\theta \sum_{n=1}^{N} g_n J_m(\delta_n r) \tag{14}$$

where the g_n are coefficients to be determined by satisfying 4(f,i). Note that (14) satisfies the pinned contact line condition 4(j) and the volume conservation condition 4(k) for non-axisymmetric ($m \neq 0$) modes. Using this representation, expressing the pressure in terms of the potential by 5(b) and projecting 4(f) and 4(i) onto the set $\{J_m(\delta_l r)\}$, we get the pair of equations

$$\sum_{n=1}^{N}(a_n\beta_{nl}^3 + b_n\xi_{nl}^3 + c_n\chi_{nl}^3) = \Omega\sum_{n=1}^{N} g_n\gamma_{nl}^3, \tag{15a}$$

$$\sum_{n=1}^{N}(a_n\beta_{nl}^4 + b_n\xi_{nl}^4 + c_n\chi_{nl}^4 + g_n\gamma_{nl}^4) = -\Omega\sum_{n=1}^{N}(a_n\beta_{nl}^5 + b_n\xi_{nl}^5 + c_n\chi_{nl}^5). \tag{15b}$$

The integrals appearing in (15) are also given in Appendix A. Using (13a,b), (15) can be written as the nonlinear eigenvalue problem

$$\mathbf{C}(\Omega; Re, Bo)\mathbf{v} = \Omega\mathbf{D}(\Omega; Re, Bo)\mathbf{v} \tag{16}$$

where $\mathbf{C}$ and $\mathbf{D}$ are $2\,N \times 2\,N$ matrices and $\mathbf{v}$ is a column vector with components $a_n, n = 1, \cdots N$ and $g_n, n = 1, \cdots N$. Note that though (16) has the formal appearance of a generalised linear eigenvalue problem, its solution requires iteration as the matrices C and D are functions of Ω. The numerical procedure consists of the following steps -

1. Start with an initial guess for Ω, Ω_i.

2. For this value of Ω and the given Re, determine the eigenvalues λ_n, μ_n and ν_n.

3. Compute the matrices C and D.

4. Solve the eigenvalue problem (16) and obtain Ω_f.

5. If $\mathrm{Re}\{\Omega_f - \Omega_i\}$ and $\mathrm{Im}\{\Omega_f - \Omega_i\} < \epsilon$ for a chosen tolerance, the calculation is done. If not, repeat (1)-(5) with $\Omega_i = \alpha_0\Omega_i + (1-\alpha_o)\Omega_f$, with $\alpha_o \in (0,1)$. We have used $\alpha_o = 0.5$.

(16) has been solved by the LAPACK routine ZGEEV. The pinned contact line frequencies for infinite depth and a flat interface (Kidambi 2007) have been used as starting values; these are then continued in the $h - \theta_c - Re - Bo$ space to the required parameter values. In general the procedure works well and convergence is achieved under ten iterations. Note that this procedure has to be repeated for the different modes i.e. even though N Ω are obtained by solving (16), all these will not be the correct values as the iteration was performed with respect to only one of those temporal eigenvalues. In other words, each modal frequency has corresponding to it a different set of spatial eigenvalues. The axisymmetric case $m = 0$ is more subtle. Now mass conservation is not automatic unlike in the non-axisymmetric case; this defines a constraint on the g_n appearing in η given by (14). However, using this and the fact that a constant term has to be included in the expansion for ϕ (Shankar 2007) leads to a similar eigenvalue problem as for the non-axisymmetric modes.

3.3 The case of finite depth

When the cylinder is of finite depth, there are three additional conditions to be satisfied on the bottom wall; this fact is reflected in an increase in the number of unknown coefficients to be determined. The velocity field in this case can be written

$$u_r(r,\theta,z) = \cos m\theta \sum_{n=1}^{\infty}\Bigg[p_n^1(r)\Big(a_n\frac{\cosh\lambda_n(z+h/2)}{\cosh\lambda_n\frac{h}{2}} + d_n\frac{\sinh\lambda_n(z+h/2)}{\sinh\lambda_n\frac{h}{2}}\Big)$$
$$+q_n^1(r)\Big(b_n\frac{\cosh\mu_n(z+h/2)}{\cosh\mu_n\frac{h}{2}} + e_n\frac{\sinh\mu_n(z+h/2)}{\sinh\mu_n\frac{h}{2}}\Big) + s_n^1(r)\Big(c_n\frac{\cosh\nu_n(z+h/2)}{\cosh\nu_n\frac{h}{2}} + f_n\frac{\sinh\nu_n(z+h/2)}{\sinh\nu_n\frac{h}{2}}\Bigg], \tag{17a}$$

$$u_\theta(r,\theta,z) = -\sin m\theta \sum_{n=1}^{\infty}\Bigg[p_n^2(r)\Big(a_n\frac{\cosh\lambda_n(z+h/2)}{\cosh\lambda_n\frac{h}{2}} + d_n\frac{\sinh\lambda_n(z+h/2)}{\sinh\lambda_n\frac{h}{2}}\Big)$$
$$+q_n^2(r)\Big(b_n\frac{\cosh\mu_n(z+h/2)}{\cosh\mu_n\frac{h}{2}} + e_n\frac{\sinh\mu_n(z+h/2)}{\sinh\mu_n\frac{h}{2}}\Big) + s_n^2(r)\Big(c_n\frac{\cosh\nu_n(z+h/2)}{\cosh\nu_n\frac{h}{2}} + f_n\frac{\sinh\nu_n(z+h/2)}{\sinh\nu_n\frac{h}{2}}\Bigg], \tag{17b}$$

$$u_z(r,\theta,z) = \cos m\theta \sum_{n=1}^{\infty}\Bigg[p_n^3(r)\Big(a_n\frac{\sinh\lambda_n(z+h/2)}{\cosh\lambda_n\frac{h}{2}} + d_n\frac{\cosh\lambda_n(z+h/2)}{\sinh\lambda_n\frac{h}{2}}\Big)$$
$$+q_n^3(r)\Big(b_n\frac{\sinh\mu_n(z+h/2)}{\cosh\mu_n\frac{h}{2}} + e_n\frac{\cosh\mu_n(z+h/2)}{\sinh\mu_n\frac{h}{2}}\Big) + s_n^3(r)\Big(c_n\frac{\sinh\nu_n(z+h/2)}{\cosh\nu_n\frac{h}{2}} + f_n\frac{\cosh\nu_n(z+h/2)}{\sinh\nu_n\frac{h}{2}}\Big)\Bigg]. \tag{17c}$$

Note that the coefficients of a_n, b_n, c_n, d_n, e_n and f_n are divided by the hyperbolic functions to keep them $O(1)$ at $z = 0$ and $z = -h$ where the boundary conditions will be applied. Projecting the shear stress condition on the interface 4(g,h) onto the complete set of functions $\{J_m(\delta_l r), l = 1, 2, \cdots\}$, we obtain the system of equations

$$\sum_{n=1}^{N}(a_n\beta_{nl}^1 + b_n\xi_{nl}^1 + c_n\chi_{nl}^1 + d_n\gamma_{nl}^1 + e_n\rho_{nl}^1 + f_n\psi_{nl}^1) = 0, \tag{18a}$$

$$\sum_{n=1}^{N}(a_n\beta_{nl}^2 + b_n\xi_{nl}^2 + c_n\chi_{nl}^2 + d_n\gamma_{nl}^2 + e_n\rho_{nl}^2 + f_n\psi_{nl}^2) = 0 \tag{18b}$$

with the various integrals given in Appendix B. The projection of the bottom boundary conditions 4(d) leads to the triple

$$\sum_{n=1}^{N}(a_n\beta_{nl}^6 + b_n\xi_{nl}^6 + c_n\chi_{nl}^6 + d_n\gamma_{nl}^6 + e_n\rho_{nl}^6 + f_n\psi_{nl}^6) = 0, \tag{19a}$$

$$\sum_{n=1}^{N}(a_n\beta_{nl}^7 + b_n\xi_{nl}^7 + c_n\chi_{nl}^7 + d_n\gamma_{nl}^7 + e_n\rho_{nl}^7 + f_n\psi_{nl}^7) = 0, \tag{19b}$$

$$\sum_{n=1}^{N}(a_n\beta_{nl}^8 + b_n\xi_{nl}^8 + c_n\chi_{nl}^8 + d_n\gamma_{nl}^8 + e_n\rho_{nl}^8 + f_n\psi_{nl}^8) = 0 \tag{19c}$$

where

$$\beta_{nl}^{6,7} = \int_0^1 rp_n^{1,2}(r)J_m(\delta_l r)dr,\ \beta_{nl}^8 = -\tanh\frac{\lambda_n h}{2}\int_0^1 rp_n^3(r)J_m(\delta_l r)dr,$$
$$\xi_{nl}^{6,7} = \int_0^1 rq_n^{1,2}(r)J_m(\delta_l r)dr,\ \xi_{nl}^8 = -\tanh\frac{\mu_n h}{2}\int_0^1 rq_n^3(r)J_m(\delta_l r)dr,$$
$$\chi_{nl}^{6,7} = \int_0^1 rs_n^{1,2}(r)J_m(\delta_l r)dr,\ \chi_{nl}^8 = -\tanh\frac{\nu_n h}{2}\int_0^1 rs_n^3(r)J_m(\delta_l r)dr,$$
$$\gamma_{nl}^{6,7} = -\beta_{nl}^{6,7},\ \rho_{nl}^{6,7} = -\xi_{nl}^{6,7},\ \psi_{nl}^{6,7} = -\chi_{nl}^{6,7}$$
$$\text{and } \gamma_{nl}^8 = -(\coth^2\lambda_n h/2)\beta_{nl}^8,\ \rho_{nl}^8 = -(\coth^2\mu_n h/2)\xi_{nl}^8 \text{ and } \psi_{nl}^8 = -(\coth^2\nu_n h/2)\chi_{nl}^8.$$

Writing (19) in matrix form as

$$\begin{aligned}
\mathbf{X_1a} + \mathbf{Y_1b} + \mathbf{Z_1c} + \mathbf{X^1d} + \mathbf{Y^1e} + \mathbf{Z^1f} &= 0,\\
\mathbf{X_2a} + \mathbf{Y_2b} + \mathbf{Z_2c} + \mathbf{X^2d} + \mathbf{Y^2e} + \mathbf{Z^2f} &= 0,\\
\mathbf{X_6a} + \mathbf{Y_6b} + \mathbf{Z_6c} + \mathbf{X^6d} + \mathbf{Y^6e} + \mathbf{Z^6f} &= 0,\\
\mathbf{X_7a} + \mathbf{Y_7b} + \mathbf{Z_7c} + \mathbf{X^7d} + \mathbf{Y^7e} + \mathbf{Z^7f} &= 0,\\
\mathbf{X_8a} + \mathbf{Y_8b} + \mathbf{Z_8c} + \mathbf{X^8d} + \mathbf{Y^8e} + \mathbf{Z^8f} &= 0
\end{aligned}$$

and defining $\mathbf{U}$ and $\mathbf{V}$ by

$$\mathbf{U} = \begin{pmatrix} \mathbf{Y_1} & \mathbf{Z_1} & \mathbf{X^1} & \mathbf{Y^1} & \mathbf{Z^1} \\ \mathbf{Y_2} & \mathbf{Z_2} & \mathbf{X^2} & \mathbf{Y^2} & \mathbf{Z^2} \\ \mathbf{Y_6} & \mathbf{Z_6} & \mathbf{X^6} & \mathbf{Y^6} & \mathbf{Z^6} \\ \mathbf{Y_7} & \mathbf{Z_7} & \mathbf{X^7} & \mathbf{Y^7} & \mathbf{Z^7} \\ \mathbf{Y_8} & \mathbf{Z_8} & \mathbf{X^8} & \mathbf{Y^8} & \mathbf{Z^8} \end{pmatrix} \text{ and } \mathbf{V} = \begin{pmatrix} \mathbf{X_1} \\ \mathbf{X_2} \\ \mathbf{X_6} \\ \mathbf{X_7} \\ \mathbf{X_8} \end{pmatrix},$$

θ_c	λ		
	$Bo = 100$	$Bo = 365$	$Bo = 1250$
30	-0.104999	-5.36708×10^{-2}	-2.86714×10^{-2}
45	-8.04986×10^{-2}	-4.11092×10^{-2}	-2.19503×10^{-2}
60	-5.45120×10^{-2}	-2.78196×10^{-2}	-1.48495×10^{-2}
75	-2.75126×10^{-2}	-1.40349×10^{-2}	-7.49016×10^{-2}

Table 1: The eigenvalue λ for $Bo = 100, 365$ and 1250 and a variety of static contact angles θ_c. $\lambda = 0$ for $\theta_c = 90^0$.

the above set of equations can be written

$$\mathbf{U} \begin{pmatrix} \mathbf{b} \\ \mathbf{c} \\ \mathbf{d} \\ \mathbf{e} \\ \mathbf{f} \end{pmatrix} = -\mathbf{V}\,\mathbf{a}$$

from which an inversion of $\mathbf{U}$ gives $\mathbf{b}, \mathbf{c}, \mathbf{d}, \mathbf{e}$ and $\mathbf{f}$ in terms of $\mathbf{a}$. Note that $\mathbf{U}$ and $\mathbf{V}$ have dimensions $5\,N \times 5\,N$ and $5\,N \times N$.

Finally, the projection of (4f,i) leads to a similar matrix eigenvalue problem as (16) which is then solved in the same way as described there. The starting values are taken as the $h = \infty$ values and the calculation proceeds by parametric continuation to lower depths (decreasing h). The axisymmetric case is very similar and will not be discussed.

4 Results & Discussion

The frequency and damping rate of a given mode depends on the four parameters Bo, Re, h and θ_c. Since the parameter space is large, we will content ourselves with calculating for a few representative cases. The static meniscus is a function of the Bond number and the contact angle and has to be first computed. We present results of the meniscus computation in §4.1. We consider the case of infinite depth in §4.2 and finally the finite depth case in §4.3.

4.1 Results for the static meniscus

The static menisci for the three Bond numbers and a variety of contact angles, for which computations will be presented, have been calculated as the first step in the calculation of Ω. 2000 eigenfunctions and 4800 minimisation points were used in the meniscus calculations. The maximum error in the satisfaction of 2(a) was of $O(10^{-5})$. The values of the eigenvalue λ for the three values of Bo and for a variety of static contact angles θ_c are presented in Table 1. Note that the λ for $\theta > 90^0$ readily follow from the fact that $\lambda(\theta_c) = -\lambda(180 - \theta_c)$.

4.2 The case of infinite depth

We present results for the case of an infinitely deep container in this section. This case is not only interesting in itself, but also provides starting values for the finite depth calculations. The results presented in this section are for $Bo = 365$ and a contact angle $\theta_c = 45^0$.

The calculations have been performed with $N = 20$ and 40 modes and with a number of different integration step sizes (used in the projection of the boundary conditions). It is found that a step size of $\Delta r = 0.01$ suffices to give convergence to five significant digits for $N = 10, 20$ whereas $\Delta r = 0.005$ is required for $N = 40$. The computations for arbitrary contact angle are continued from the computations for $\theta_c = 90^0$ (flat interface). The bottom wall boundary conditions are satisfied to $O(10^{-10})$ and the convergence criterion for the iterative procedure of §3.2, ϵ has been fixed at 10^{-6}.

Table 2 shows the frequency and damping rates for calculations with $N = 20$ and 40 modes for $Bo = 365$ and $\theta_c = 45^0$ for the $(1,0), (2,0), (3,0)$ and $(4,0)$ modes. The damping rates and frequencies have converged to two and three significant figures respectively in most cases. Since the modes under consideration are the 'viscous modes', the complex modal frequencies should approach the inviscid values as $Re \to \infty$. The inviscid values for the same Bond number and contact angle are $1.438, 1.887, 2.257$ and 2.592 respectively. These have been obtained by a procedure outlined in Shankar (2007).

4.3 The case of finite depth

In this section, we present results which show the effect of the static contact angle on the frequency and damping rates. Since the parameter space is four dimensional for each mode, it will not be possible to cover even a substantial portion of the space. The flat interface case, for which extensive experimental results (Howell et al 2000) and computational results (Martel et al 1998, Nicolás 2002) exist, was considered in Kidambi (2007). In §4.3.1, we present results for some of the cases in Howell et al (2000), but with curved static menisci, for possible comparison with future experiments. For the case of a meniscus (non - 90 contact angle), the only experimental result that we are aware of is due to Cocciaro et al (1993) who measure the frequency and damping rate of the first non-axisymmetric mode on a free surface which when static makes a contact angle $\theta_c = 62^0$. We compare the values from the present computation with the experimental values from Cocciaro et al (1993) in §4.3.2. Where appropriate, we make contact with the numerical results of Shankar (2007) and Nicolás (2005) which however only give the frequencies, being inviscid calculations.

4.3.1 Some results for possible comparison with future experiments

In this section, we present results of calculations using some of the parameters in the experiments of Howell et al (2000), but with curved static menisci. 70 different experiments were performed by Howell et al; since we have to consider each of these cases for a variety of contact angles, we will only present results for a few representative values of the Reynolds number for each mode. In particular, we present results for the highest and lowest experimetal Re for each of the six modes at the two depths of $h = 1.379$ and $h = 0.231$.

Before we go ahead and discuss the results, we review a few well-known facts about the frequency and damping rate in the cases of a free-end and pinned-end contact line. This will provide a framework for understanding the present results. The restoring force in a surface wave results from (i) the action of gravity on the displaced fluid and (ii) stretching of the free surface, the

C	$-\Omega_r$		Ω_i	
	$N=20$	$N=40$	$N=20$	$N=40$
(1,0) mode				
5×10^{-5}	0.0057	0.0053	1.436	1.434
1×10^{-4}	0.0078	0.0075	1.434	1.432
5×10^{-4}	0.0192	0.0195	1.426	1.424
1×10^{-3}	0.0306	0.0313	1.421	1.423
5×10^{-3}	0.0943	0.0952	1.395	1.393
1×10^{-2}	0.1588	0.1607	1.378	1.376
(2,0) mode				
5×10^{-5}	0.0091	0.0083	1.883	1.881
1×10^{-4}	0.0126	0.0123	1.881	1.878
5×10^{-4}	0.0335	0.0336	1.867	1.867
1×10^{-3}	0.0542	0.0585	1.860	1.859
5×10^{-3}	0.1804	0.1815	1.816	1.813
1×10^{-2}	0.3074	0.3079	1.778	1.776
(3,0) mode				
5×10^{-5}	0.0125	0.0111	2.252	2.249
1×10^{-4}	0.0175	0.0169	2.248	2.245
5×10^{-4}	0.0506	0.0486	2.231	2.229
1×10^{-3}	0.0811	0.0812	2.221	2.219
5×10^{-3}	0.2811	0.2821	2.152	2.150
1×10^{-2}	0.4765	0.4766	2.080	2.078
(4,0) mode				
5×10^{-5}	0.0159	0.0141	2.587	2.583
1×10^{-4}	0.0227	0.0219	2.582	2.578
5×10^{-4}	0.0695	0.0665	2.561	2.559
1×10^{-3}	0.1116	0.1122	2.547	2.543
5×10^{-3}	0.3946	0.3974	2.446	2.442
1×10^{-2}	0.6614	0.6654	2.327	2.325

Table 2: The frequencies and damping rates of the $(1,0),(2,0),(3,0),(4,0)$ modes by using $N=20$ and 40 spatial modes. The static contact angle $\theta_c = 45^0$.

k_n	3.832	7.016	10.173	13.324	16.471
l_n	1.841	5.331	8.536	11.706	14.864

Table 3: The first few permissible wavenumbers for pinned contact line (k_n) and free contact line (l_n). Inviscid flow is assumed.

two forces coming into play being gravity and surface tension. The gravitational contribution is directly proportional to the free surface displacement η which in turn is directly proportional to the vertical component of velocity on the free surface $u_z - \eta_s^{'} u_r$. The capillary contribution is directly proportional to the free surface curvature and inversely proportional to the Bond number Bo. It is well known that u_z is directly proportional to the wavenumber k which in turn is related to the edge conditions and also to the depth. Thus we have the following -

1. Higher modes, which by definition have higher wave number, have higher frequencies.

2. For a fixed mode, the frequency decreases with decreasing depth.

3. Pinned contact lines result in higher frequencies than free end ones. This is directly related to the magnitudes of the wavenumbers that are allowed in the two cases. Considering the inviscid situation for simplicity, η satisfies $\eta(r = 1) = 0$ and $\eta^{'}(r = 1) = 0$ in the two cases respectively. [1]For a fixed mode with mode number m, this leads to the eigenvalue relations $J_m(k_n) = 0$ and $J_m^{'}(l_n) = 0$ respectively. Again, it is well known that $k_n > l_n$ for given n. The first few k_n and l_n for $m = 1$ are given in Table 3. It is clear that $\omega_{pc} > \omega_{fc}$ where the subscripts refer to the pinned and free contact lines.

4. The frequency increases with the contact angle θ_c for $\theta_c \in [0, \pi]$ in the free end case (Kidambi & Shankar 2004, Nicolás 2005). If the contact line is pinned, the frequency increases with increasing θ_c only for $\theta_c < \theta_c^o$ [2]; beyond this, it decreases. This behaviour is different from the free end case.

5. The frequency increases with decreasing Bo. This is because of an increased capillary contribution to the springiness of the free surface.

The effects of viscosity on the frequency are felt through the no-slip boundary condition on the walls and through the Re term in the dynamic boundary condition on the free surface. The viscous effect is the classical one that obtains in the damped spring-mass system; the frequency reduces with increasing viscosity (or decreasing Re), slowly for high Re and more rapidly for lower values till at $Re = Re_{cr}$ it goes to zero. For $Re < Re_{cr}$, the critical Reynolds number, the frequency remains zero resulting in an overdamped system (Nicolás 2002, Kidambi 2007).

The factors contributing to the damping rate are more subtle. One straightforward correlation is with the velocity gradients; the steeper the gradients, the higher the damping. Thus, we have

[1]In the free end case, the boundary condition can only be prescribed for the velocity potential ϕ. However, if the contact angle $\theta_c = 90^0$, this condition translates to the one given above for η. For $\theta_c \neq 90^0$, this condition is still valid if η is taken as the departure from the static meniscus (Kidambi & Shankar 2004).

[2]Nicolás (2005) and Shankar (2007) differ in the value of θ_c^o; for Nicolás $\theta_c^o = 90^0$ with attendant symmetry about this value whereas Shankar's results show no symmetry and the peak is at $\theta_c^o \approx 95^0$ for the paricular parameter values considered. Note that Nicolás (2005) is an asymptotic result valid for $Bo \to \infty$ whereas Shankar (2007) solves an inviscid eigenvalue problem valid for all Bond numbers.

θ_c	$-\Omega_r$						Ω_i					
	(1,0)	(2,0)	(0,1)	(3,0)	(1,1)	(4,0)	(1,0)	(2,0)	(0,1)	(3,0)	(1,1)	(4,0)
150	0.0030	0.0037	0.0046	0.0055	0.0049	0.0079	1.414	1.858	2.063	2.215	2.479	2.538
135	0.0039	0.0056	0.0046	0.0079	0.0062	0.0106	1.427	1.878	2.075	2.242	2.494	2.571
120	0.0047	0.0074	0.0046	0.0101	0.0072	0.0129	1.437	1.895	2.084	2.266	2.507	2.601
105	0.0056	0.0090	0.0047	0.0118	0.0077	0.0143	1.444	1.907	2.089	2.282	2.515	2.621
90	0.0063	0.0098	0.0047	0.0124	0.0079	0.0150	1.446	1.912	2.090	2.289	2.516	2.629
75	0.0067	0.0099	0.0049	0.0127	0.0080	0.0157	1.444	1.909	2.086	2.285	2.511	2.626
60	0.0066	0.0100	0.0051	0.0133	0.0083	0.0168	1.436	1.898	2.078	2.271	2.499	2.609
45	0.0066	0.0105	0.0053	0.0144	0.0087	0.0184	1.423	1.879	2.064	2.247	2.481	2.580
30	0.0069	0.0114	0.0052	0.0160	0.0093	0.0208	1.407	1.855	2.048	2.216	2.459	2.542

Table 4: The damping rate and frequency (Ω_r^t, Ω_i^t) of the lowest six modes as a function of the static contact angle. $Re = 13077.02, h = 1.379$ and $Bo = 365$ as in the experiments of Howell et al (2000) for the $\theta_c = 90^0$ case.

1. Higher modes have higher damping. Velocity gradients are proportional to wavenumbers and higher modes have larger wavenumbers.
2. Damping increases with decreasing depth.

We also briefly recall the primary contributions to viscous damping, from the asymptotic analysis of Martel et al (1998). In particular, we recall the forms of Ω_r^{t*} and Ω_i^{t*}, the theoretical damping rate and frequency as being

$$\Omega_r^{t*} = a_1 C^{1/2} + a_2 C, \Omega_i^{t*} = a_0 - a_1 C^{1/2}.$$

The $O(1)$ inviscid solution gives a_0, $a_1 C^{1/2}$ describes the first approximation to viscous dissipation in the Stokes layers near the walls and $a_2 C$ includes the effects of the bulk viscous dissipation as well as a higher order correction to the damping in the Stokes layers. To the level of approximation computed by Martel et al, the effects of the free surface boundary layer are not included at all, even for a flat interface. The presence of a meniscus may result in the free surface boundary layer dissipation contributing at lower order.

We also recall a similar (in spirit) asymptotic analysis by Nicolás (2005) which takes into account the static meniscus but in an inviscid setting. The small parameter in this analysis is the inverse of the Bond number; the analysis for the pinned contact line condition shows that the frequency, to first order, is an even function of $90^0 - \theta_c$ and that the frequency for the flat interface is the maximum. Being an inviscid analysis, no direct calculation of the damping rate is possible.

With this as background, we now look at the present results. Table 4 shows the frequency and damping rates for all six modes for a Reynolds number of 13077.02 and nine contact angles ranging from 30^0 to 150^0. The frequency variation follows the trend in Nicolás (2005) and Shankar (2007), with a peak in the neighbourhood of 90^0. The damping rates of all modes except $(1, 0)$ and $(0, 1)$ also vary according to the predictions made in the previous paragraph,

θ_c	$-\Omega_r$						Ω_i					
	(1,0)	(2,0)	(0,1)	(3,0)	(1,1)	(4,0)	(1,0)	(2,0)	(0,1)	(3,0)	(1,1)	(4,0)
150	0.0712	0.1205	0.1208	0.1024	0.1082	0.0728	1.381	1.807	2.036	2.195	2.469	2.533
135	0.0686	0.1223	0.1229	0.1042	0.1094	0.0743	1.394	1.828	2.047	2.214	2.478	2.556
120	0.0672	0.1238	0.1246	0.1066	0.1108	0.0761	1.405	1.845	2.057	2.233	2.487	2.578
105	0.0670	0.1258	0.1263	0.1093	0.1122	0.0781	1.412	1.856	2.062	2.245	2.493	2.594
90	0.0677	0.1283	0.1249	0.1122	0.1133	0.0804	1.414	1.859	2.062	2.249	2.493	2.600
75	0.0691	0.1315	0.1266	0.1154	0.1143	0.0830	1.411	1.856	2.058	2.243	2.487	2.596
60	0.0714	0.1362	0.1291	0.1194	0.1156	0.0861	1.402	1.843	2.050	2.228	2.476	2.579
45	0.0756	0.1423	0.1333	0.1248	0.1175	0.0899	1.389	1.833	2.035	2.206	2.460	2.554
30	0.0809	0.1485	0.1339	0.1315	0.1202	0.0942	1.374	1.822	2.016	2.181	2.444	2.524

Table 5: The damping rate and frequency (Ω_r^t, Ω_i^t) of the lowest six modes as a function of the static contact angle. $Re = 272.48, 271.44, 269.91, 568.51, 570.78$ and 1323.45 for the $(1,0), (2,0), (0,1), (3,0), (1,1)$ and $(4,0)$ modes respectively. These values are the lowest Reynolds numbers in the experiments of Howell et al (2000) for the $\theta_c = 90^0$ case. $h = 1.379, Bo = 365$.

increasing with decreasing θ_c i.e. decreasing mean depth. The damping rate of the $(1,0)$ mode also follows the expected trend for $\theta_c > 75^0$ but for θ_c below this, it does not vary appreciably. The damping rate of the $(0,1)$ mode though following expected trends, shows a variation only in the fourth decimal for $\theta_c > 120^0$; in general the variation over the whole range of θ_c is much less compared to the other modes. Table 5 shows similar values for the lowest experimental Reynolds numbers; again except for the $(1,0)$ and $(0,1)$ modes, the frequency and damping rates follow the expected trends. For the $(1,0)$ mode, the damping rate has a minimum around 90^0 while the damping rate for the $(0,1)$ mode has a local maximum around 105^0. The reason for these anomalies is not known.

Table 6 shows the frequencies and damping rates for a $Bo = 1250$, a shallow depth of $h = 0.231$ and the highest experimental $Re = 32819.17$. This small liquid depth case shows an interesting result - the frequency peak in the neighbourhood of 90^0 that was seen for the larger depth disappears and the frequency now monotonically increases as the contact angle increases for all the modes except $(4,0)$ which shows a peak frequency around 120^0. . The damping rates, on the other hand, follow the predicted trends increasing with decreasing contact angle. The frequency variation with θ_c is counter to the predictions in Nicolás (2005) and Shankar (2007), both of which predict a frequency maximum in the neighbourhood of 90^0; however, the calculations in these cases were for $h = 1$ even though for Nicolás, the size of h would probably not alter the trend. To be confident of the present results, we have done two calculations -

- Solve the inviscid eigenvalue problem for the same parameters and examine if the inviscid frequencies also follow this trend.
- Calculate the inviscid frequencies for the parameters considered by Nicolás (2005) (and plotted in fig 4 of his paper) and compare.

The results of these calculations for the $(1,0)$ and $(4,0)$ modes are shown in Table 7. The

θ_c	$-\Omega_r$						Ω_i					
	(1,0)	(2,0)	(0,1)	(3,0)	(1,1)	(4,0)	(1,0)	(2,0)	(0,1)	(3,0)	(1,1)	(4,0)
150	0.0068	0.0081	0.0071	0.0086	0.0054	0.0088	0.922	1.459	1.744	1.896	2.230	2.260
135	0.0076	0.0088	0.0074	0.0094	0.0058	0.0096	0.916	1.457	1.736	1.895	2.225	2.264
120	0.0083	0.0097	0.0077	0.0103	0.0064	0.0106	0.908	1.448	1.726	1.892	2.219	2.267
105	0.0090	0.0105	0.0080	0.0113	0.0070	0.0117	0.899	1.438	1.713	1.885	2.210	2.264
90	0.0093	0.0114	0.0084	0.0124	0.0077	0.0129	0.887	1.423	1.696	1.872	2.196	2.254
75	0.0098	0.0121	0.0088	0.0134	0.0084	0.0142	0.873	1.405	1.677	1.853	2.179	2.236
60	0.0100	0.0127	0.0157	0.0143	0.0092	0.0154	0.858	1.383	1.662	1.828	2.157	2.212
45	0.0102	0.0132	0.0217	0.0153	0.0099	0.0168	0.841	1.358	1.644	1.800	2.133	2.183
30	0.0103	0.0137	0.0364	0.0161	0.0106	0.0181	0.825	1.334	1.569	1.771	2.109	2.151

Table 6: The damping rate and frequency (Ω_r^t, Ω_i^t) of the lowest six modes as a function of the static contact angle. $Re = 32819.17, h = 0.231$ and $Bo = 1250$ as in the experiments of Howell et al (2000) for the $\theta_c = 90^0$ case.

θ	$Bo = 1250$		$Bo = 100$	$m = 4$
	$h = 0.231$	$h = 1$		
150	0.927	1.359	1.498	2.263
135	0.921	1.365	1.500	2.270
120	0.915	1.370	1.522	2.274
105	0.906	1.374	1.535	2.272
95	0.899	1.375	1.538	2.267
90	0.895	1.375	1.537	2.264
75	0.882	1.374	1.528	2.248
60	0.867	1.369	1.508	2.225
45	0.850	1.363	1.477	2.197
30	0.834	1.356	1.466	2.166

Table 7: The inviscid frequencies of the $(1, 0)$ and $(4, 0)$ modes. $Bo = 1250$ and 100 for the $m = 1$ mode. At $h = 0.231$, the frequencies increase monotonically with θ_c unlike at $h = 1$. where there is a peak around 90^0. For $Bo = 100$ and $h = 1$. (second last column), the frequency peak has shifted away from 90^0. For the $m = 4$ mode, $Bo = 1250$ and $h = 0.231$.

θ_c	$-\Omega_r$						Ω_i					
	(1,0)	(2,0)	(0,1)	(3,0)	(1,1)	(4,0)	(1,0)	(2,0)	(0,1)	(3,0)	(1,1)	(4,0)
150	0.0725	0.1637	0.1554	0.1289	0.2139	0.0936	0.875	1.374	1.688	1.847	2.180	2.231
135	0.0738	0.1678	0.1596	0.1320	0.2182	0.0952	0.868	1.367	1.678	1.839	2.171	2.227
120	0.0754	0.1727	0.1643	0.1357	0.2233	0.0972	0.859	1.358	1.666	1.830	2.161	2.223
105	0.0774	0.1782	0.1699	0.1399	0.2291	0.0996	0.849	1.345	1.651	1.818	2.148	2.215
90	0.0796	0.1843	0.1761	0.1447	0.2357	0.1024	0.836	1.328	1.633	1.801	2.131	2.202
75	0.0819	0.1908	0.1827	0.1498	0.2430	0.1058	0.821	1.307	1.611	1.779	2.111	2.183
60	0.0845	0.1979	0.1901	0.1553	0.2512	0.1094	0.804	1.282	1.586	1.752	2.088	2.159
45	0.0871	0.2057	0.1982	0.1610	0.2601	0.1136	0.788	1.255	1.560	1.724	2.063	2.131
30	0.0898	0.2138	0.2069	0.1665	0.2693	0.1169	0.769	1.228	1.533	1.695	2.038	2.103

Table 8: The damping rate and frequency (Ω_r^t, Ω_i^t) of the lowest six modes as a function of the static contact angle. $Re = 676.13, 337.84, 337.84, 673.85, 337.84$ and 1433.90 for the $(1,0), (2,0), (0,1), (3,0), (1,1)$ and $(4,0)$ modes respectively. These values are the lowest Reynolds numbers in the experiments of Howell et al (2000) for the $\theta_c = 90^0$ case. $h = 0.231, Bo = 1250$.

numbers in the first column confirm that the inviscid frequencies also are monotonic with respect to the contact angle. If Shankar (2007) had chosen to calculate for this depth, this is what he would have obtained. The third column shows the numbers for a case that Nicolás (2005) has calculated; $Bo = 100$ and $h = 1$. Though Nicolás' result (eq. 56 of his paper) shows symmetry about 90^0 with a peak there, the present calculation shows a peak around 95^0 which is probably a result of the small $Bo = 100$; to confirm this, results were generated for $Bo = 1250$, shown in the second column, which confirms that the peak has substantially shifted towards 90^0. We recall that Nicolás' asymptotic analysis is expected to be increasingly in error as the Bond number reduces and more terms are required. Thus, it is not surprising that the results for $Bo = 1250$ are in closer agreement than the ones for $Bo = 100$. What is surprising is that Nicolás' asymptotic results do not seem to correctly predict the frequency behaviour for shallow depth ($h = 0.231$); they continue to predict symmetry with a peak at 90^0 whereas a direct calculation shows monotonic behaviour as the values in the first column indicate. The numbers in the last column for the $(4,0)$ mode indicate that the small depth is not sufficient to cause the monotonic behaviour of the frequency with contact angle. Results for the lowest experimental Reynolds number at this depth and Bond number are shown in Table 8. The trends are similar to those at the higher Reynolds number (table 6). Note that the damping rates of the $(1,0)$ and $(0,1)$ modes also follow the expected trends for these parameter values.

We now explore the variation of the frequency and the damping rate of the $(1,0)$ mode with depth for a variety of $\theta_c; Bo = 1250$ as before and we choose an $Re = 676.13$, one of the experimental values in Howell et al (2000). Table 9 shows these variations for depths ranging from 0.3 to 0.7. At the lower depths, the damping rate monotonically decreases with contact angle but develops a minimum whose location shifts towards 90^0 for increasing depth. On the other hand, the frequency monotonically increases with increasing θ_c at lower depths but develops a maximum whose location again shifts towards 90^0 for increasing depth. Tables 10 -12 present results for some regions of the parameter space that Howell et al (2000) does not cover.

θ_c	$-\Omega_r$	Ω_i	$-\Omega_r$	Ω_i
h = 0.3			h = 0.4	
150	.0615	0.978	.0522	1.092
135	.0619	0.974	.0521	1.091
120	.0627	0.969	.0523	1.089
105	.0639	0.962	.0528	1.085
90	.0652	0.952	.0536	1.078
75	.0667	0.940	.0546	1.070
60	.0683	0.926	.0558	1.059
45	.0702	0.911	.0571	1.048
30	.0720	0.896	.0588	1.034
h = 0.5			h = 0.6	
150	.0470	1.173	.0440	1.236
135	.0464	1.174	.0432	1.236
120	.0462	1.175	.0427	1.236
105	.0465	1.173	.0427	1.236
90	.0469	1.169	.0430	1.234
75	.0477	1.163	.0437	1.229
60	.0488	1.154	.0447	1.222
45	.0499	1.146	.0458	1.215
30	.0510	1.138	.0468	1.209
h = 0.7			h = 1.379	
150	.0426	1.271	.0416	1.357
135	.0413	1.275	.0396	1.364
120	.0406	1.279	.0385	1.370
105	.0405	1.281	.0381	1.375
90	.0407	1.279	.0382	1.376
75	.0413	1.276	.0387	1.375
60	.0422	1.270	.0397	1.372
45	.0434	1.264	.0411	1.366
30	.0443	1.259	.0428	1.360

Table 9: The damping rate and frequency of the $(1, 0)$ mode for various shallow depths and one large depth. $Re = 676.13$ and $Bo = 1250$.

$\theta_c(^0)$	150	135	120	105	90	75	60	45	30
$-\Omega_r$	.0046	.0055	.0061	.0066	.0069	.0071	.0071	.0069	.0066
Ω_i	1.382	1.387	1.392	1.395	1.396	1.394	1.391	1.385	1.379

Table 10: Variation of damping rate and frequency with θ_c for the $(1,0)$ mode. $Re = 13077.02, Bo = 1250, h = 1.379$.

$\theta_c(^0)$	150	135	120	105	90	75	60	45	30
$-\Omega_r$	.0109	.0118	.0127	.0137	.0147	.0157	.0166	.0176	.0185
Ω_i	0.976	0.967	0.955	0.938	0.916	0.889	0.858	0.824	0.789

Table 11: Variation of damping rate and frequency with θ_c for the $(1,0)$ mode. $Re = 13077.02, Bo = 365, h = 0.231$.

The variation of the frequency and damping rate for the high $Re = 13077.02, Bo = 1250$ and $h = 1.379$ is presented in Table 10; the frequency variation is similar as for the lower $Bo = 365$ (Table 4) but the damping rate shows subtle differences. The results for a high $Re = 13077.02$ and a low $Bo = 365$ and $h = 0.231$ are shown in Table 11; the damping rates (frequencies) decrease (increase) monotonically with increasing θ_c. Table 12 shows similar behaviour of these quantities for the low $Re = 272.48, Bo = 365$ and $h = 0.231$.

Asymptotic inviscid calculations (eq. 56) of Nicolás (2005) show that, for a fixed depth, the frequency increases with a decrease in Bond number. Table 13 shows the frequencies and damping rates for $Bo = 1250$ and $Bo = 365$ at a fixed depth of $h = 0.3$. Though at $\theta_c > 45^0$ the frequency at the lower Bond number is higher, the trend is different at $\theta_c < 45^0$. This shows that the meniscus effect can be dominant for small contact angles even reversing the effects due to an increased surface tension effect.

For ease of visualisation, some of these results have been graphed in figures 2 - 4. Figure 2 shows the effect of depth with $Re = 13077.02, Bo = 365$. For the smaller depth (Table 11), the damping rate decreases monotonically with increasing θ_c whereas at the larger depth, a local maximum occurs around 75^0 (Table 4). Figure 2(b) shows the variation of the frequency with θ_c; at the smaller depth, the frequency increases monotonically with θ_c (free-end behaviour) while at the larger depth, a maximum occurs around 90^0 (pinned-end behaviour).

Figure 3 shows the effect of Re with $Bo = 365$ and $h = 1.379$. The damping rate at the lower Re has a minimum around 105^0 (Table 5)in contrast to the local maximum around 75^0 (Table 4) for the higher Re. The frequencies however show similar trends attaining maxima around 90^0. The effect of the Bond number is shown in figure 4. The damping rate for the higher Bo (Table 10) has a global maximum around 75^0 in contrast to the local maximum around the same θ_c for the lower Bond number. $Re = 13077.02$ and $h = 1.379$. The frequencies show similar trends though the overall variation is much smaller at the higher Bond number.

$\theta_c(^0)$	150	135	120	105	90	75	60	45	30
$-\Omega_r$	.1265	.1286	.1329	.1394	.1476	.1576	.1695	.1837	.2007
Ω_i	0.912	0.899	0.885	0.864	0.839	0.809	0.775	0.737	0.698

Table 12: Variation of damping rate and frequency with θ_c for the $(1,0)$ mode. $Re = 272.48, Bo = 365, h = 0.231$.

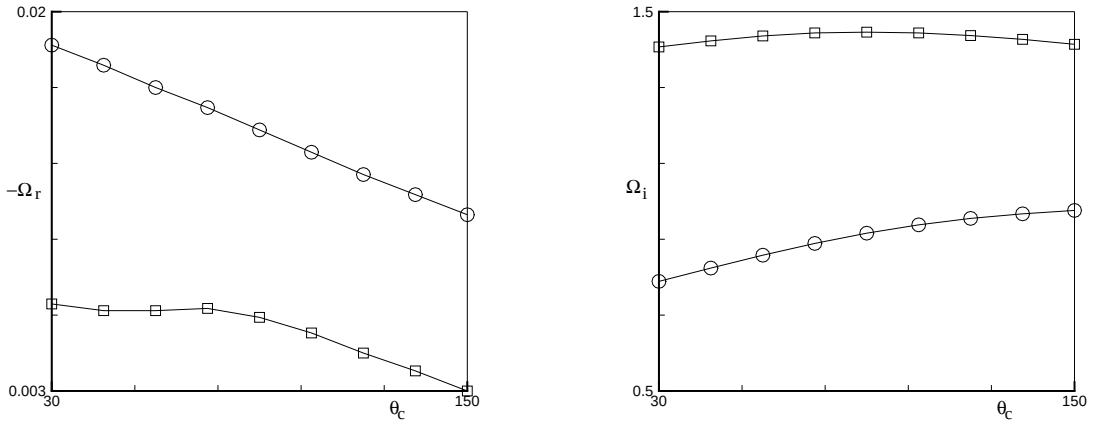

(a) (b)

Figure 2: Variation of (a) damping rate and (b) frequency of the (1,0) mode for $\circ$, $h = 0.231$ and $\square$ $h = 1.379. Bo = 365, Re = 13077.02$.

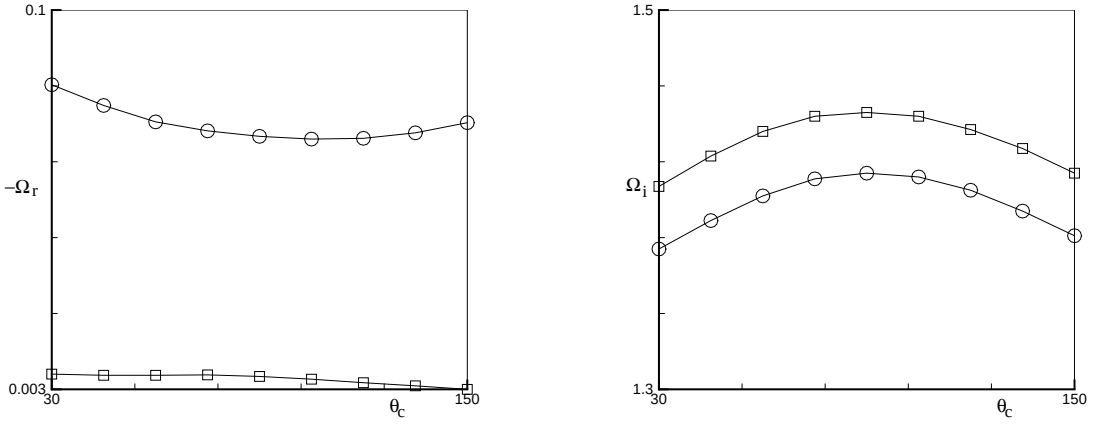

(a) (b)

Figure 3: Variation of (a) damping rate and (b) frequency of the (1,0) mode for $\circ$, $Re = 272.48$ and $\square$ $h = 13077.02. Bo = 365, h = 1.379$.

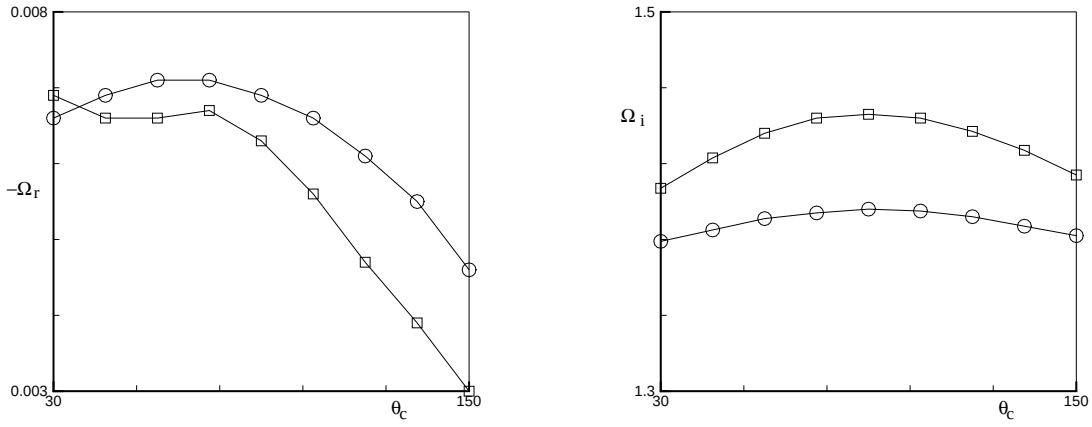

(a) (b)

Figure 4: Variation of (a) damping rate and (b) frequency of the (1,0) mode for $\circ$, $Bo = 1250$ and $\square$ $Bo = 365. Re = 13077.02, h = 1.379$.

θ	$-\Omega_r$		Ω_i	
	$Bo = 365$	$Bo = 1250$	$Bo = 365$	$Bo = 1250$
150	.0604	.0615	1.035	0.978
135	.0600	.0619	1.030	0.974
120	.0609	.0627	1.022	0.969
105	.0628	.0639	1.008	0.962
90	.0653	.0652	0.989	0.952
75	.0682	.0667	0.967	0.940
60	.0713	.0684	0.939	0.926
45	.0746	.0702	0.908	0.911
30	.0782	.0720	0.875	0.896

Table 13: The frequencies and damping rates of the $(1, 0)$ mode at $h = 0.3$ for $Bo = 365$ and 1250. Note that for $\theta < 45^0$, the frequencies at the higher $Bo = 1250$ are greater than those at $Bo = 365$ contrary to the trend for $\theta > 45^0$.

Re	$-\Omega_r$	Ω_i	$-\Omega_r$	Ω_i	$-\Omega_r$	Ω_i
$\underline{\theta_c = 150^0}$			$\underline{\theta_c = 135^0}$			$\underline{\theta_c = 120^0}$
25	1.438	1.561	1.442	1.564	1.447	1.564
24	1.476	1.514	1.479	1.517	1.484	1.517
23	1.263	1.187×10^{-3}	1.271	4.890×10^{-4}	1.272	2.705×10^{-3}
$\underline{\theta_c = 105^0}$			$\underline{\theta_c = 90^0}$			$\underline{\theta_c = 75^0}$
25	1.453	1.560	1.461	1.551	1.435	1.586
24	1.489	1.512	1.275	1.662×10^{-3}	1.217	6.547×10^{-4}
23	1.262	2.582×10^{-4}	-	-	-	-
$\underline{\theta_c = 60^0}$			$\underline{\theta_c = 45^0}$			$\underline{\theta_c = 30^0}$
30 (33,35)	1.335	1.719	1.281	1.796	1.251	1.842
29 (32,34)	1.360	1.688	1.301	1.771	0.957	2.229×10^{-4}
28 (31)	1.387	1.655	1.068	7.551×10^{-5}	-	-
27 (30)	1.129	5.084×10^{-5}	-	–	-	-

Table 14: The frequencies and damping rates of the $(4, 0)$ mode at $h = 1.5$ for $Bo = 365$ and a few Re near Re_{crit}. The values for $Re < Re_{cr}$ are not shown. The bracketed numbers in the first column correspond to $\theta_c = 45^0$ and 30^0 respectively.

$\theta_c(^0)$	150	135	120	105	90	75	60	45	30
Re_{cr}	23	23	23	23	24	24	27	31	34

Table 15: Variation of Re_{cr} with θ_c for the $(4, 0)$ mode. $h = 1.5$ and $Bo = 365$.

It is known (Nicolás 2002, Kidambi 2007) that there exists a critical Reynolds number, Re_{crit} below which the frequency vanishes. Re_{crit} increases with increasing mode number, increases with decreasing depth and increases with decreasing Bond number, with all other parameters being held constant in each case. We now examine how Re_{crit} depends on the contact angle for fixed Bo, h and m; calculations are presented for $Bo = 365, h = 1.5$ and $m = 4$. Table 14 shows the frequency and damping rate for a variety of θ_c for a few values near Re_{cr}. Table 15 shows the variation of Re_{cr} with θ_c. For $\theta_c < 90^0, Re_{cr}$ increases with decreasing θ_c while for $\theta_c > 90^0, Re_{cr} \approx 23$ irrespective of θ_c. The same trends are expected to hold at lower depths; the Re_{cr} values will be higher than the present values as the frequencies are lower.

4.3.2 Comparison with the experiment of Cocciaro et al (1993)

Cocciaro et al (1993) measured the frequency and damping rate of the first non-axisymmetric mode $(1, 0)$ in a cylindrical container where the free surface makes a static contact angle $\theta_c = 62^0$ with the vertical walls. Two regimes of contact line motion were identified; one of these was found to be a small oscillation amplitudes regime where the contact line remained at rest.

N	$-\Omega_r$	Ω_i
20	3.767×10^{-3}	1.452
40	3.659×10^{-3}	1.452

Table 16: The non-dimensional damping rate and frequency of the $(1, 0)$ mode using 20 and 40 modes. $Re = 35628.103, Bo = 346.363$ and $h = 2.587$. The static contact angle $\theta_c = 62^0$. These values are same as those used in the experiment of Cocciaro et al (1993).

The damping rate and frequency in this regime were measured to be $\gamma = 15 \pm 2mHz$ and $\nu = 3.222 \pm 0.001Hz$. Miles' theory (1991), which neglects the static meniscus, gives an inviscid frequency estimate of 3.255 Hz; a viscous correction following Hocking (1987a,b) further refines this value to 3.249 Hz. Note that Hocking's results were obtained for a rectangular geometry; Cocciaro et al (1993) assume that these still hold good for a cylindrical geometry. Cocciaro et al speculate that meniscus effects could account for the discrepancy of $27mHz$; this is borne out by a recent calculation in Shankar (2007) which includes the meniscus effects and produces a value of $3.224Hz$. The Hocking calculation, which also neglects static meniscus effects, produces a damping rate of $12mHz$ which is somewhat lower than the experimental value. Cocciaro et al consider the possibility that this discrepancy could be due to the presence of a residual surface contaminating film; however, a calculation with such a film produces a damping rate of $30mHz$ which is double the experimental value.

We have calculated the frequency and damping rate for this case by the present method. Using values of $R = 5.025\,cm, H = 13\,cm, g = 980.5cm/s^2$, kinematic viscosity $\nu_c = 0.0099cm^2/s$ and capillary length $\lambda_c = 2.7\,mm$, we have the Reynolds and Bond numbers as 35628.103 and 346.363 respectively. Table 16 shows the damping rate and frequency for these parameters obtained using 20 and 40 modes.

The dimensional variables ν and γ in Cocciaro et al (1993) are related to the present non-dimensional variables Ω_i and Ω_r as

$$2\pi\nu = \sqrt{g/R}\,\Omega_i, \pi\gamma = \sqrt{g/R}\,\Omega_r.$$

Using the 40 mode values in the above expressions yields values of $3.228Hz$ and $16.27mHz$ for the frequency and damping rate; these compare very well with the experimental values of $3.222 \pm 0.001Hz$ and $15 \pm 2mHz$ respectively.

Nicolás (2005) has estimated the frequency and damping rate for this case. He represents the static meniscus as an asymptotic expansion and uses the first two terms, unlike in the present case where it is numerically evaluated. A first order approximation for the frequency which was first given by Miles (1991) and higher order corrections given by Martel et al (1998), which do not include meniscus effects, are used to produce a frequency of $3.222Hz$ and a damping rate of $14.65mHz$, numbers closer to the experimental values than the present ones. However, the present calculation is exact unlike Nicolás (2005) which uses various approximations.

5 Conclusion

We have presented a new eigenvalue formulation for the calculation of damping rates and natural frequencies of surface capillary-gravity waves in a circular cylinder with pinned contact line,

with meniscus effects considered for the first time. This formulation uses the Helmholtz decomposition for the velocity field with the complex vector eigenfunctions of the unsteady Stokes operator in a cylindrical geometry generated from the satisfaction of the no-slip condition on the sidewall (Kidambi 2007) where extensive comparisons with available experimental (Howell et al 2000, Cocciaro et al 1993) and computational (Nicolás 2002) results, for the no-meniscus case, show excellent agreement.

For $\theta_c \neq 90^0$ but fixed, the variation of the frequency and the damping rate with Re, Bo, h and m follow broadly the same patterns as for $\theta_c = 90^0$. Thus, for fixed Bo, m and $h(Re)$, the frequency decreases and the damping rate increases with decreasing $Re(h)$. For fixed Bo, Re and h, the frequency and damping rate increase with m. For fixed Re, h and m, the frequency increases with decreasing Bo; the damping rate is only weakly dependent on Bo showing a slight increase with decreasing Bo. However, for small h and large menisci (small θ_c), we can have (table 13) the frequency decreasing with decreasing Bo while the damping rates exhibit a mixed trend - decreasing for $\theta_c > 90^0$ and increasing otherwise, with decreasing Bo. Thus, the meniscus makes a qualitative difference only for small contact angles and small depths.

A study of the variation of the frequency and damping rate with θ_c reveals different behaviours depending on Re, Bo, h and m. The frequency can exhibit, depending on the various parameters, either a monotonic increase or a maximum with increasing θ_c whereas the damping rate can exhibit a monotonic decrease, a maximum or a minimum. For shallow depths, the damping rate and frequency exhibit, in general, behaviour that is similar to that reported for free contact lines (Henderson et al 1992, Kidambi & Shankar 2004, Nicolás 2005); the former decreases and the latter increases monotonically with θ_c. This seems to be true irrespective of the values of Re and Bo. However, the frequency of the $(4, 0)$ mode shows a peak around $\theta_c = 120^0$ for $Re = 32819.17$ and $Bo = 1250$ (table 6) though it follows the usual trend for the lower $Re = 1433.90$ (table 8). The behaviour for large depth is also equally interesting. For large depths and higher modes, the damping rate monotonically increases for decreasing θ_c while the frequency exhibits a maximum in the neighbourhood of 90^0. The frequency behaviour is similar to the inviscid behaviours of the pinned contact line reported in Nicolás (2005) and Shankar (2007) and is different from the behaviour for free contact lines (Henderson et al 1992, Kidambi & Shankar 2004, Nicolás 2005) where the frequency increases monotonically with increasing θ_c. A systematic calculation of the damping rate for the free contact line case is not available, for comparison. However, the damping rate of the $(1, 0)$ and $(0, 1)$ modes does not decrease monotonically for any of the parameter values considered. Instead, it can exhibit a maximum (table 4 - $(0, 1)$ mode, table 10) or minimum (tables 5 and 9 - $(1, 0)$ mode) or both a maximum and a minimum (table 4 - $(1, 0)$ mode, table 5 - $(0, 1)$ mode) depending on the values of Re and Bo. A gradual change from the non-monotonic to the monotonic behaviour can be seen as the depth decreases. The critical Reynolds number, Re_{cr} increases with decreasing θ_c, all other parameters being constant. An asymptotic analysis on the lines of Martel et al (1998), but with a meniscus present, is needed to delineate the different effects especially at high Re and Bo. The present formulation can be easily adapted to consider the effects of surface contamination, elastic covers, microgravity conditions etc. These problems are being studied and will be reported elsewhere.

Acknowledgments
The work is funded by the Aeronautical Reserarch & Development Board, India under project No. 1031340. I also thank Dr. P. N. Shankar for a careful reading of the manuscript and valuable suggestions.

Appendix A

The integrals appearing in equations (12) and (15) are given below.

$$\beta^1_{nl} = \int_0^1 r\Bigg\{(\eta_s^{'2}-1)\bigg(\lambda_n p^1_n(r) + \frac{dp^3_n(r)}{dr}\bigg) + 2\eta_s^{'}\bigg(\frac{dp^1_n(r)}{dr} - \lambda_n p^3_n(r)\bigg)\Bigg\}e^{\lambda_n\eta_s(r)}J_m(\delta_l r)dr,$$

$$\beta^2_{nl} = \int_0^1 r\Bigg\{\lambda_n p^2_n(r) + \frac{m}{r}p^3_n(r) - \eta_s^{'}\bigg(\frac{m}{r}p^1_n(r) - \frac{p^2_n(r)}{r} + \frac{dp^2_n(r)}{dr}\bigg)\Bigg\}e^{\lambda_n\eta_s(r)}J_m(\delta_l r)dr,$$

$$\xi^1_{nl} = \int_0^1 r\Bigg\{(\eta_s^{'2}-1)\bigg(\mu_n q^1_n(r) + \frac{dq^3_n(r)}{dr}\bigg) + 2\eta_s^{'}\bigg(\frac{dq^1_n(r)}{dr} - \mu_n q^3_n(r)\bigg)\Bigg\}e^{\mu_n\eta_s(r)}J_m(\delta_l r)dr,$$

$$\xi^2_{nl} = \int_0^1 r\Bigg\{\mu_n q^2_n(r) + \frac{m}{r}q^3_n(r) - \eta_s^{'}\bigg(\frac{m}{r}q^1_n(r) - \frac{q^2_n(r)}{r} + \frac{dq^2_n(r)}{dr}\bigg)\Bigg\}e^{\mu_n\eta_s(r)}J_m(\delta_l r)dr,$$

$$\chi^1_{nl} = \int_0^1 r\Bigg\{(\eta_s^{'2}-1)\bigg(\nu_n s^1_n(r) + \frac{ds^3_n(r)}{dr}\bigg) + 2\eta_s^{'}\bigg(\frac{ds^1_n(r)}{dr} - \nu_n s^3_n(r)\bigg)\Bigg\}e^{\nu_n\eta_s(r)}J_m(\delta_l r)dr,$$

$$\chi^2_{nl} = \int_0^1 r\Bigg\{\nu_n s^2_n(r) + \frac{m}{r}s^3_n(r) - \eta_s^{'}\bigg(\frac{m}{r}s^1_n(r) - \frac{s^2_n(r)}{r} + \frac{ds^2_n(r)}{dr}\bigg)\Bigg\}e^{\nu_n\eta_s(r)}J_m(\delta_l r)dr,$$

$$\beta^3_{nl} = \int_0^1 re^{\lambda_n\eta_s(r)}(p^3_n - \eta_s^{'}p^1_n)J_m(\delta_l r)dr,\ \xi^3_{nl} = \int_0^1 re^{\mu_n\eta_s(r)}(q^3_n - \eta_s^{'}q^1_n)J_m(\delta_l r)dr,$$

$$\chi^3_{nl} = \int_0^1 re^{\nu_n\eta_s(r)}(s^3_n - \eta_s^{'}s^1_n)J_m(\delta_l r)dr,\ \gamma^3_{nl} = \int_0^1 rJ_m(\delta_n r)J_m(\delta_l r)dr,$$

$$\beta^4_{nl} = \frac{2}{Re}\int_0^1 \frac{re^{\lambda\eta_s(r)}}{1+\eta_s^{'2}}\bigg[\lambda_n p^3_n(r) - \eta_s^{'}(\lambda_n p^1_n(r) + \frac{dp^3_n(r)}{dr}) + \eta_s^{'2}p^1_n(r)\bigg]J_m(\delta_l r)dr,$$

$$\xi^4_{nl} = \frac{2}{Re}\int_0^1 \frac{re^{\mu\eta_s(r)}}{1+\eta_s^{'2}}\bigg[\mu_n q^3_n(r) - \eta_s^{'}(\mu_n q^1_n(r) + \frac{dq^3_n(r)}{dr}) + \eta_s^{'2}q^1_n(r)\bigg]J_m(\delta_l r)dr,$$

$$\chi^4_{nl} = \frac{2}{Re}\int_0^1 \frac{re^{\nu\eta_s(r)}}{1+\eta_s^{'2}}\bigg[\nu_n s^3_n(r) - \eta_s^{'}(\nu_n s^1_n(r) + \frac{ds^3_n(r)}{dr}) + \eta_s^{'2}s^1_n(r)\bigg]J_m(\delta_l r)dr,$$

$$\gamma^4_{nl} = \int_0^1 r\bigg[\frac{\delta_n^2 r^2 + m^2\eta_s^{'2}}{r^2(1+\eta_s^{'2})^{3/2}}J_m(\delta_n r) - \bigg(\frac{3\eta_s^{'2}}{r(1+\eta_s^{'2})^{3/2}} - \delta_n\frac{3\eta_s^{'}\kappa_s}{1+\eta_s^{'2}}\bigg)\frac{J_{m-1}(\delta_n r) - J_{m+1}(\delta_n r)}{2}\bigg]J_m(\delta_l r)dr,$$

$$\beta^5_{nl} = \int_0^1 re^{\lambda_n\eta_s(r)}J_m(\lambda_n r)J_m(\delta_l r)dr,\ \xi^5_{nl} = \int_0^1 re^{\mu_n\eta_s(r)}J_m(\mu_n r)J_m(\delta_l r)dr,$$

$$\chi^5_{nl} = \int_0^1 re^{\nu_n\eta_s(r)}J_m(\nu_n r)J_m(\delta_l r)dr.$$

Appendix B

We list here the various integrals that appear in §3.3.

$$\beta^1_{nl} = \int_0^1 r\left\{(\eta_s^{'2}-1)\left(\lambda_n p^1_n(r) + \frac{dp^3_n(r)}{dr}\right) + 2\eta_s^{'}\left(\frac{dp^1_n(r)}{dr} - \lambda_n p^3_n(r)\right)\right\}\frac{\sinh\lambda_n(\eta_s(r)+h/2)}{\cosh\frac{\lambda_n h}{2}}J_m(\delta_l r)dr,$$

$$\beta^2_{nl} = \int_0^1 r\left\{\lambda_n p^2_n(r) + \frac{m}{r}p^3_n(r) - \eta_s^{'}\left(\frac{m}{r}p^1_n(r) - \frac{p^2_n(r)}{r} + \frac{dp^2_n(r)}{dr}\right)\right\}\frac{\sinh\lambda_n(\eta_s(r)+h/2)}{\cosh\frac{\lambda_n h}{2}}J_m(\delta_l r)dr,$$

$$\xi^1_{nl} = \int_0^1 r\left\{(\eta_s^{'2}-1)\left(\mu_n q^1_n(r) + \frac{dq^3_n(r)}{dr}\right) + 2\eta_s^{'}\left(\frac{dq^1_n(r)}{dr} - \mu_n q^3_n(r)\right)\right\}\frac{\sinh\mu_n(\eta_s(r)+h/2)}{\cosh\frac{\mu_n h}{2}}J_m(\delta_l r)dr,$$

$$\xi^2_{nl} = \int_0^1 r\left\{\mu_n q^2_n(r) + \frac{m}{r}q^3_n(r) - \eta_s^{'}\left(\frac{m}{r}q^1_n(r) - \frac{q^2_n(r)}{r} + \frac{dq^2_n(r)}{dr}\right)\right\}\frac{\sinh\mu_n(\eta_s(r)+h/2)}{\cosh\frac{\mu_n h}{2}}J_m(\delta_l r)dr,$$

$$\chi^1_{nl} = \int_0^1 r\left\{(\eta_s^{'2}-1)\left(\nu_n s^1_n(r) + \frac{ds^3_n(r)}{dr}\right) + 2\eta_s^{'}\left(\frac{ds^1_n(r)}{dr} - \nu_n s^3_n(r)\right)\right\}\frac{\sinh\mu_n(\eta_s(r)+h/2)}{\cosh\frac{\mu_n h}{2}}J_m(\delta_l r)dr,$$

$$\chi^2_{nl} = \int_0^1 r\left\{\nu_n s^2_n(r) + \frac{m}{r}s^3_n(r) - \eta_s^{'}\left(\frac{m}{r}s^1_n(r) - \frac{s^2_n(r)}{r} + \frac{ds^2_n(r)}{dr}\right)\right\}\frac{\sinh\nu_n(\eta_s(r)+h/2)}{\cosh\frac{\nu_n h}{2}}J_m(\delta_l r)dr,$$

$$\gamma^1_{nl} = \int_0^1 r\left\{(\eta_s^{'2}-1)\left(\lambda_n p^1_n(r) + \frac{dp^3_n(r)}{dr}\right) + 2\eta_s^{'}\left(\frac{dp^1_n(r)}{dr} - \lambda_n p^3_n(r)\right)\right\}\frac{\cosh\lambda_n(\eta_s(r)+h/2)}{\sinh\frac{\lambda_n h}{2}}J_m(\delta_l r)dr,$$

$$\gamma^2_{nl} = \int_0^1 r\left\{\lambda_n p^2_n(r) + \frac{m}{r}p^3_n(r) - \eta_s^{'}\left(\frac{m}{r}p^1_n(r) - \frac{p^2_n(r)}{r} + \frac{dp^2_n(r)}{dr}\right)\right\}\frac{\cosh\lambda_n(\eta_s(r)+h/2)}{\sinh\frac{\lambda_n h}{2}}J_m(\delta_l r)dr,$$

$$\rho^1_{nl} = \int_0^1 r\left\{(\eta_s^{'2}-1)\left(\mu_n q^1_n(r) + \frac{dq^3_n(r)}{dr}\right) + 2\eta_s^{'}\left(\frac{dq^1_n(r)}{dr} - \mu_n q^3_n(r)\right)\right\}\frac{\cosh\mu_n(\eta_s(r)+h/2)}{\sinh\frac{\mu_n h}{2}}J_m(\delta_l r)dr,$$

$$\rho^2_{nl} = \int_0^1 r\left\{\mu_n q^2_n(r) + \frac{m}{r}q^3_n(r) - \eta_s^{'}\left(\frac{m}{r}q^1_n(r) - \frac{q^2_n(r)}{r} + \frac{dq^2_n(r)}{dr}\right)\right\}\frac{\cosh\mu_n(\eta_s(r)+h/2)}{\sinh\frac{\mu_n h}{2}}J_m(\delta_l r)dr,$$

$$\psi^1_{nl} = \int_0^1 r\left\{(\eta_s^{'2}-1)\left(\nu_n s^1_n(r) + \frac{ds^3_n(r)}{dr}\right) + 2\eta_s^{'}\left(\frac{ds^1_n(r)}{dr} - \nu_n s^3_n(r)\right)\right\}\frac{\cosh\mu_n(\eta_s(r)+h/2)}{\sinh\frac{\mu_n h}{2}}J_m(\delta_l r)dr,$$

$$\psi^2_{nl} = \int_0^1 r\left\{\nu_n s^2_n(r) + \frac{m}{r}s^3_n(r) - \eta_s^{'}\left(\frac{m}{r}s^1_n(r) - \frac{s^2_n(r)}{r} + \frac{ds^2_n(r)}{dr}\right)\right\}\frac{\cosh\nu_n(\eta_s(r)+h/2)}{\sinh\frac{\nu_n h}{2}}J_m(\delta_l r)dr.$$

References

[1] Benjamin, T.B. & Scott, J.C. 1979 Gravity - capillary waves with edge constraints. *J. Fluid Mech.* 92, 241 - 267.

[2] Cocciaro, B., Faetti, S. & Festa, C. 1993 Experimental investigation of capillarity effects on surface gravity waves : non-wetting boundary conditions. *J. Fluid Mech.* 246, 43 - 66.

[3] Henderson, D.M., Hammack, J., Kumar, P. & Shah, D. 1992 The effects of static contact angles on standing waves. *Phys. Fluids A* 4, 2320 - 2322.

[4] Henderson, D.M. & Miles, J.W. 1994 Surface-wave damping in a circular cylinder with a fixed contact line. *J. Fluid Mech.* 275, 285 - 299.

[5] Hocking, L.M. 1987a The damping of capillary-gravity waves at a rigid boundary. *J. Fluid Mech.* 179, 253 - 266.

[6] Hocking, L.M. 1987b Waves produced by a vertically oscillating plate. *J. Fluid Mech.* 179, 267 - 281.

[7] Howell, D.R., Buhrow. B., Heath, T., McKenna, C., Hwang, W. & Schatz, M.F., 2000 Measurements of surface-wave damping in a container. *Phys. Fluids* 12(2), 322 - 326.

[8] Johnson, R.S. 1997 A modern introduction to the mathematical theory of water waves. *Camb. Univ. Press*

[9] Kidambi, R. & Shankar, P.N. 2004 The effects of the contact angle on sloshing in containers. *Proc. R. Soc. Lond. A* 460, 2251 - 2267.

[10] Kidambi, R. 2006 Oscillatory eddy structure in a cylindrical container. *Fluid Dyn. Res.* 38, 274 - 294.

[11] Kidambi, R. 2007 Oscillations of a viscous free surface with pinned contact line. *Fluid Dyn. Res.* 39, 121 - 138.

[12] Kidambi, R. 2007 Damping of capillary - gravity waves in a brimful circular cylinder. *PD CF 0706*

[13] Martel, C., Nicolás, J.A. & Vega, J.M. 1998 Surface-wave damping in a brimful circular cylinder. *J. Fluid Mech.* 360, 213 - 228.

[14] Miles, J.W. 1991 The capillary boundary layer for standing waves. *J. Fluid Mech.* 222, 197 - 205.

[15] Miles, J.W. & Henderson, J.M. 1998 A note on interior vs. boundary- layer damping of surface waves in a circular cylinder. *J. Fluid Mech.* 364, 319 - 323.

[16] Morse, P.M. & Feshbach, H., 1953 Methods of theoretical physics. Part 2. *McGraw-Hill, New York.*

[17] Nicolás, J.A. 2002 The viscous damping of capillary-gravity waves in a brimful circular cylinder. *Phys. Fluids* 14, 1910 - 1919.

[18] Nicolás, J.A. 2005 Effects of static contact angles on inviscid gravity-capillary waves. *Phys. Fluids* 17, 022101.

[19] Perlin, M., Schultz, W.W. & Liu, Z. 2004 High Reynolds number oscillating contact lines. *Wave Motion* 40, 41 - 56.

[20] Shankar, P.N. 2007 Frequencies of gravity - capillary waves on highly curved interfaces with edge constraints. *Fluid Dyn. Res.* 39, 457 - 474.